Research
A SCIENCE PARTNER JOURNAL

REVIEW ARTICLE

Advances in Catalysts for Magnesium-Based Hydrogen Storage Materials

Yong Zhu[1,2,3†], Wenhao Ma[2†], Xingzai Chai[2], Yunpeng Gu[2], Wenqi Wu[2], Haisheng Chen[2,3,4*], and Ting Zhang[2,3,4,5*]

[1]School of Energy and Mechanical Engineering, Nanjing Normal University, Nanjing 210042, China. [2]Nanjing Institute of Future Energy System, Nanjing 211135, China. [3]University of Chinese Academy of Sciences, Nanjing 211135, China. [4]University of Chinese Academy of Sciences, Beijing 100049, China. [5]Institute of Engineering Thermophysics, Chinese Academy of Sciences, Beijing 100190, China.

*Address correspondence to: chen_hs@iet.cn (H.C.); zhangting@iet.cn (T.Z.)
†These authors contributed equally to this work.

Citation: Zhu Y, Ma W, Chai X, Gu Y, Wu W, Chen H, Zhang T. Advances in Catalysts for Magnesium-Based Hydrogen Storage Materials. *Research* 2025;8:Article 1036. https://doi.org/10.34133/research.1036

Submitted 6 August 2025
Revised 26 November 2025
Accepted 27 November 2025
Published 22 December 2025

Copyright © 2025 Yong Zhu et al. Exclusive licensee Science and Technology Review Publishing House. No claim to original U.S. Government Works. Distributed under a Creative Commons Attribution License (CC BY 4.0).

MgH_2 (magnesium hydride) has attracted attention as a potential hydrogen storage material owing to its rich availability and high theoretical hydrogen capacity. Nevertheless, its practical utilization is restricted by its high thermodynamic stability and slow hydrogen sorption kinetics. Recent advancements have demonstrated that incorporating various catalytic systems—such as transition metals, metal oxides, metal halides, metal sulfides, and carbon-supported materials—effectively improves hydrogen dissociation, diffusion, and Mg–H bond modulation. Structural transformations, interfacial interactions, and synergistic effects in multicomponent systems substantially enhance MgH_2 performance. Furthermore, cutting-edge computational techniques such as DFT (density functional theory) and ML (machine learning) have become indispensable for expediting catalyst development and forecasting their performance. These computational techniques enable high-throughput screening, provide atomic-scale insights into catalytic mechanisms, and substantially reduce experimental workloads. This review systematically summarizes recent progress in catalytic modifications of MgH_2, elucidates the underlying enhancement mechanisms, highlights the contributions of DFT and ML methodologies, and discusses future directions such as nanostructuring, multifunctional composite catalysts, and computational-driven rational catalyst design for next-generation hydrogen storage technologies.

Introduction

Solid-state hydrogen storage has emerged as a safe and efficient alternative to conventional hydrogen storage methods [1–4]. Among diverse solid-state materials, metal hydrides stand out due to their notable advantages, including high hydrogen storage densities and reversible hydrogen absorption and desorption capacities. In particular, MgH_2 (magnesium hydride) has gained growing attention due to its abundant natural availability and impressive theoretical hydrogen storage capacity of 7.6 wt% [5–8].

Nonetheless, the widespread use of MgH_2 is severely limited by its substantial thermodynamic stability and slow kinetics during hydrogenation and dehydrogenation processes. For example, the hydrogenation/dehydrogenation reaction has an enthalpy of approximately 75 kJ/mol. Consequently, the desorption temperature under atmospheric pressure is around 311 °C, which far exceeds the practical range for most applications. Moreover, because magnesium lacks d orbitals, it interacts weakly with the σ* antibonding orbitals of H_2. As a result, H_2 dissociates slowly on the Mg surface. Additionally, surface oxidation [e.g., MgO and $Mg(OH)_2$ layers] further hampers hydrogen diffusion. Effective hydrogen storage is therefore limited to elevated temperature and pressure.

To overcome these challenges, several optimization strategies, such as nanoscaling, alloying, and catalytic modification, have been proposed [9–12]. Among these strategies, catalytic modification is particularly effective. It promotes H_2 dissociation, accelerates atomic hydrogen diffusion, and tunes the stability of Mg–H bonds, thereby improving the kinetics of MgH_2 [13].

A wide range of catalysts—including transition metals and their alloys, metal oxides, metal halides, metal sulfides, and carbon-supported materials—show substantial promise for improving MgH_2 performance. Representative examples are summarized in Fig. 1. Some magnesium-based hydrogen storage materials already meet the DOE (U.S. Department of Energy) 2025 targets for hydrogen storage quality and refueling rate but remain somewhat distant in terms of cost and cycle life.

This review systematically examines recent advancements in catalytic systems applied to MgH_2-based hydrogen storage. Initially, the intrinsic physicochemical characteristics and hydrogen storage mechanisms of MgH_2 are described. Subsequently, we explore catalytic mechanisms associated with various catalyst types and analyze their impacts on the hydrogen storage properties. Finally, drawing on existing studies, we outline the remaining challenges and future research avenues. Our aim is to provide

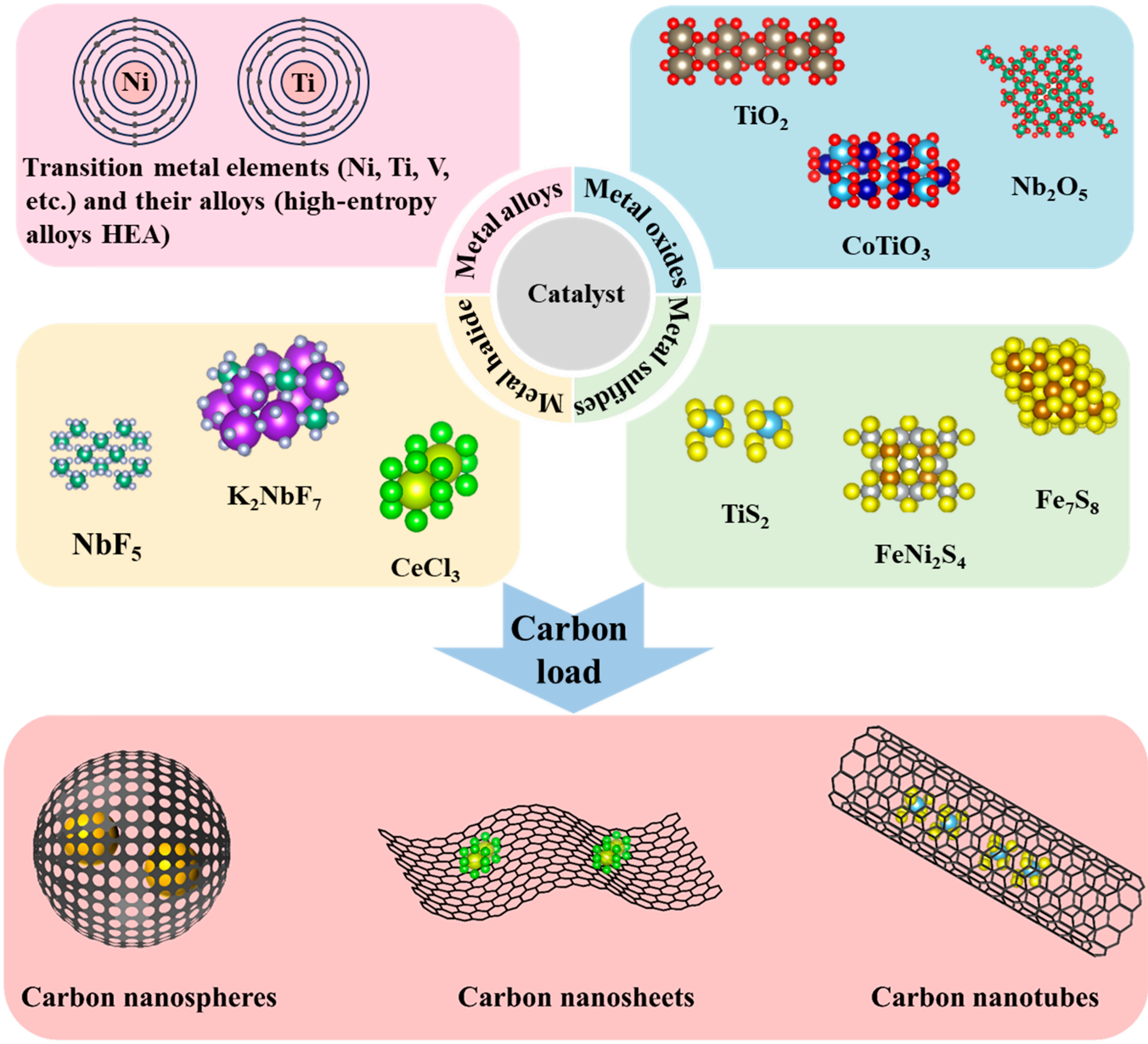


Fig. 1. Commonly used catalyst types for MgH_2 hydrogen storage.

theoretical insight and practical guidance for advancing high-performance hydrogen storage materials.

Catalytic Mechanism of Hydrogen Storage in MgH_2

Hydrogen storage in MgH_2 is a reversible solid–gas reaction: under suitable temperature and H_2 pressure, magnesium forms the hydride (Eq. 1).

$$Mg + H_2 \leftrightarrow MgH_2 \qquad \Delta H = 75 \ \text{kJ/mol} \tag{1}$$

This exothermic reaction is reversible and can be driven in either direction by adjusting the temperature and the partial pressure of hydrogen. The mechanism proceeds in stages: (a) physisorption of H_2 on the surface followed by dissociation; (b) chemisorption and surface diffusion of H atoms; and (c) incorporation into the Mg lattice, where MgH_2 nucleates and grows. Conversely, dehydrogenation must overcome a substantial activation energy. Its kinetics are limited by the formation of hydrogen vacancies and the cleavage of Mg–H bonds [14].

Thermodynamically, the dehydrogenation reaction of MgH_2 is characterized by an enthalpy change (ΔH) of approximately 75 kJ/mol and an entropy change (ΔS) of about 130 $J \cdot K^{-1} \cdot mol^{-1}$, as described by the van't Hoff equation (Eq. 2):

$$\ln P = \frac{\Delta H}{RT} - \frac{\Delta S}{R} \tag{2}$$

where P is the equilibrium hydrogen pressure, T is the absolute temperature, R is the ideal gas constant (8.314 $J \cdot mol^{-1} \cdot K^{-1}$), and ΔH and ΔS are the enthalpy and entropy changes of the dehydrogenation reaction, respectively.

The equilibrium dehydrogenation temperature is approximately 311 °C at standard atmospheric pressure, indicating a substantial thermodynamic barrier to hydrogen desorption

under conventional operating conditions [15]. To address the thermodynamic and kinetic challenges, incorporating catalysts has emerged as an essential approach to improve the hydrogen storage capability of MgH_2.

Appropriate catalysts can greatly enhance the rates of hydrogen absorption and desorption by reducing the energy barrier for H_2 dissociation, promoting the surface diffusion of hydrogen atoms, and adjusting the stability of Mg–H bonds [16,17]. By Sabatier's principle, an effective catalyst should bind hydrogen moderately—strong enough to dissociate H_2 but weak enough to avoid retaining H atoms—so that hydrogen transfers smoothly into the Mg matrix.

During the reaction, some catalysts can undergo in situ transformation into highly active intermediate phases, such as metal hydrides, alloys, or nanometal clusters. These intermediates often provide additional hydrogen diffusion pathways or reduce the binding energy of Mg–H bonds [18]. In addition, interfacial effects—such as the hydrogen spillover phenomenon and hydrogen pumping mechanism—are pivotal to both hydrogen absorption and desorption, substantially improving the overall kinetic performance. To analyze the kinetics of hydrogen absorption and desorption, models such as the JMAK (Johnson–Mehl–Avrami–Kolmogorov) model and diffusion-controlled models are commonly employed, offering insights into the rate-determining steps and catalytic pathways.

Metal and Alloy Catalysts

The d orbitals of transition metals possess relatively high energy levels that are closely aligned with the σ* antibonding orbitals of hydrogen molecules. This energetic compatibility facilitates effective orbital interactions, which weaken the H–H bonds and subsequently lower the energy barrier for hydrogen dissociation [19]. The metal and alloy catalysts involved in this article are shown in Table S1.

Initial investigations into enhancing the dynamics of MgH_2 centered on single-element catalysts. For instance, Yan et al. [20] reported that nano-Mn catalysts substantially reduced the onset dehydrogenation temperature of MgH_2 from 355 to 175 °C and decreased the activation energy for hydrogenation from 72.5 to 18.8 kJ/mol. Furthermore, 6.7 wt% of hydrogen was desorbed within 5 min at 300 °C, with 92% capacity retention after 20 cycles. The enhancement was attributed to the stable dispersion of nano-Mn, which provided interfacial active sites and facilitated hydrogen diffusion. Nevertheless, nanoparticle agglomeration and surface oxidation during cycling remain critical barriers to long-term durability. To overcome these drawbacks, attention has shifted toward SACs (single-atom catalysts), which maximize atomic utilization and interfacial reactivity. Yang et al. [21] developed an alloy-type Mo SAC (Mo_1-MgH_2) by loading $Mo(CO)_6$ onto MgH_2 via impregnation and in situ activation. The synthesized Mo_1–MgH_2 composite demonstrated a marked decrease in the onset desorption temperature to 218 °C, along with a lowered activation energy for dehydrogenation at 110 kJ/mol. It absorbed 6.77 wt% H_2 within 1 min (Fig. 2B) and desorbed over 5.0 wt% within 150 min at 250 °C (Fig. 2C), while maintaining nearly 100% capacity after 10 cycles. These improvements were attributed to the atomic-scale integration of Mo with MgH_2, which enabled efficient hydrogen adsorption, dissociation, and diffusion, as well as facilitated Mg–H bond cleavage during dehydrogenation (Fig. 2A). However, robustly anchoring metals as isolated single atoms at defect or coordination sites requires stringent control of precursors, atmosphere, and temperature, which substantially elevates costs. Moreover, maintaining comparable defect densities and uniform dispersion during scale-up is difficult, thereby hindering large-scale manufacturing.

Compared with single-element catalysts, multimetal alloys offer tunable electronic structures and cooperative interfacial chemistry. Yang et al. [22] synthesized FeCo nanosheets via wet chemical methods and investigated their catalytic effect in the MgH_2 system. The composites exhibited a reduced dehydrogenation temperature range of 200 to 320 °C and desorbed 6 wt% hydrogen in 9.5 min at 300 °C. The activation energy was lowered to 65.3 kJ/mol. The Fe–Co bimetallic system offered numerous active sites for H_2 dissociation and facilitated hydrogen spillover onto the MgH_2 surface, thereby greatly improving the kinetics of hydrogen storage. However, potential risks still exist regarding the compositional segregation of Fe/Co and the morphological stability of ultrathin nanosheets during cycling.

In contrast, compared with conventional binary and ternary alloys, HEAs (high-entropy alloys) and MEAs (medium-entropy alloys) offer superior structural and thermal stability, as well as enhanced catalytic activity. Wan et al. [23] demonstrated that doping MgH_2 with 5 wt% FeCoNiCrMn HEA enabled the adsorption of 5.5 wt% hydrogen within 0.5 min at 150 °C (Fig. 2E) and the desorption of 5.8 wt% hydrogen within 4 min at 280 °C (Fig. 2F), with a reduced dehydrogenation activation energy of 90.2 kJ/mol. Furthermore, its hydrogen storage capacity remained at 98.6% after 50 cycles, far exceeding that of most similar catalysts. However, this still falls short of the cycle life specified in the 2025 DOE's target. This improvement was mainly attributed to the synergistic catalytic effect of the multiple elements in the HEA, which facilitated both hydrogen dissociation and the rapid cleavage of Mg–H bonds (Fig. 2D). Furthermore, Jiang et al. [24] synthesized an amorphous FeCoNiLa MEA via pulsed electrodeposition and used it as a catalyst for MgH_2. Doping MgH_2 with 10 wt% FeCoNiLa enabled the desorption of 6.5 wt% hydrogen within 5 min at 325 °C (Fig. 2H) and reduced the dehydrogenation activation energy from 159.3 to 103.9 kJ/mol. It also facilitated rapid hydrogen absorption, with 6 wt% absorbed within 1 min at 275 °C (Fig. 2I). The composite maintained 98.2% of its initial capacity after 20 cycles. The enhanced performance was attributed to the multiphase synergistic catalysis of FeCoNiLa and in situ formed Co_3Fe_7, as well as the reversible Mg_2Ni/Mg_2NiH_4 phase, which contributed a hydrogen pumping effect, together facilitating Mg–H bond dissociation and hydrogen diffusion (Fig. 2G). However, obtaining a near-atomic single-phase solid solution typically requires high-purity metals and energy-intensive processing, which results in manufacturing costs exceeding the DOE's target of $9/kWh.

To reduce production costs, some research has turned to economical and environmentally friendly synthetic methods, aiming to achieve similar kinetics with simpler chemical reactions and lower processing burden. Huang et al. [25] developed a mechanochemical synthesis method for highly dispersed Ni–N–C composites using simple ball milling, pyrolysis, and aqueous washing, without relying on large quantities of organic solvents. When applied to MgH_2, the catalyst facilitated hydrogen desorption of 5.4 wt% within 5 min at 300 °C and lowered the activation energy for dehydrogenation to 87.2 kJ/mol. This improvement was mainly ascribed to the highly electronegative sites within the Ni–N–C framework, which effectively enhanced hydrogen molecule dissociation. In addition, Machmud and Jalil [26]

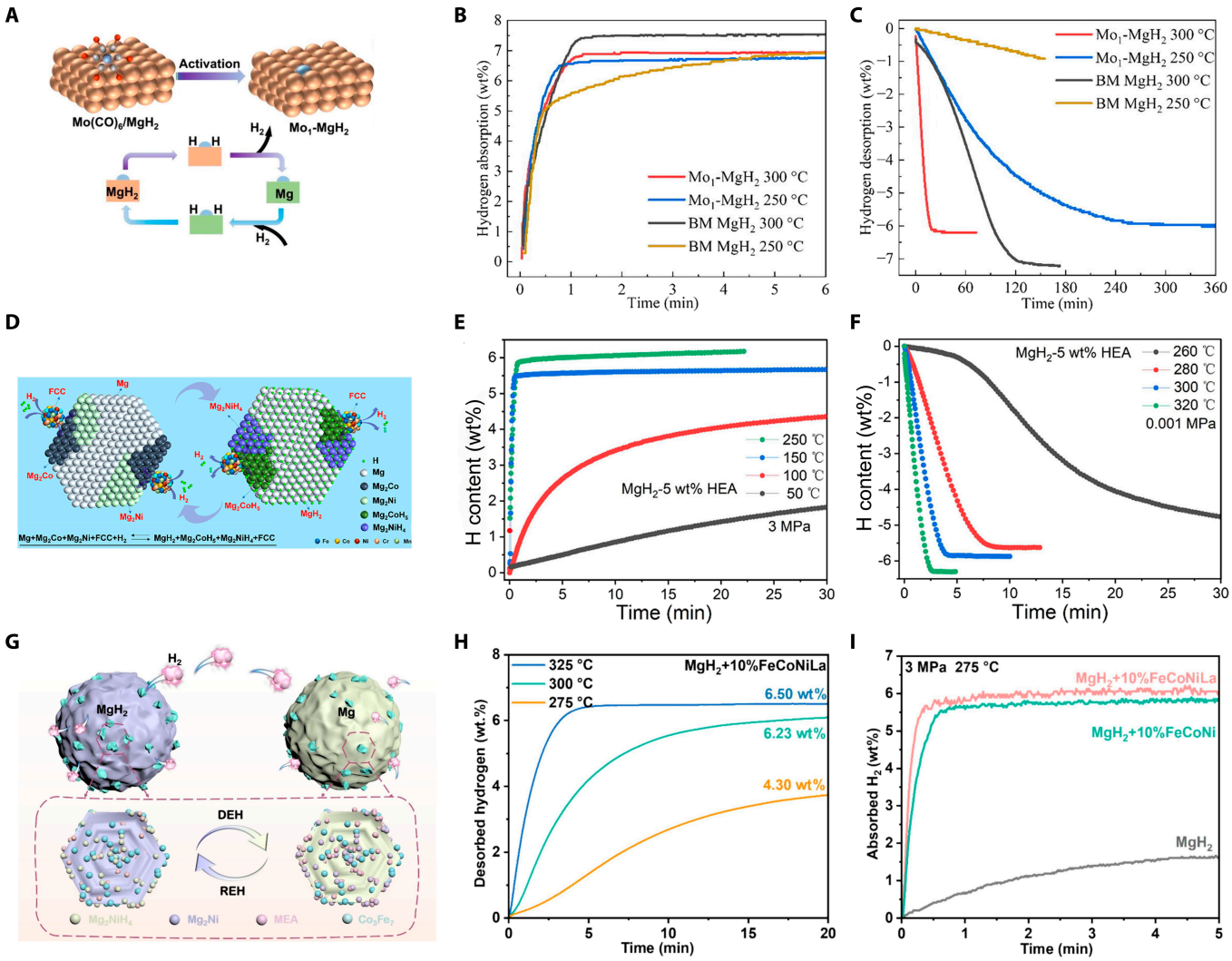


Fig. 2. (A) Schematics of the hydrogenation and dehydrogenation mechanisms of MgH_2 doped with Mo_1. (B) Hydrogenation profiles and (C) corresponding dehydrogenation profiles of MgH_2 doped with Mo_1 at different temperatures [21]. (D) Schematics of the hydrogenation and dehydrogenation mechanisms of MgH_2 doped with HEA. (E) Hydrogenation profiles and (F) corresponding dehydrogenation profiles of MgH_2 doped with 5 wt% HEA at different temperatures [23]. (G) Schematics of the hydrogenation and dehydrogenation mechanisms of MgH_2 doped with FeCoNiLa. (H) Dehydrogenation behavior of MgH_2 doped with 10 wt% FeCoNiLa at different temperatures. (I) Hydrogenation behavior of MgH_2 doped with 10 wt% FeCoNi and FeCoNiLa catalysts at 275 °C under 3 MPa [24].

prepared Ti-doped MgH_2 composites using HPRM (high-pressure reactive ball milling). The introduction of Ti nanoparticles effectively suppressed Mg grain growth and substantially lowered the activation energies for both hydrogenation and dehydrogenation, with complete dehydrogenation achieved in just 6 min at 350 °C. Similarly, Rahwanto et al. [27] synthesized MgH_2 composites doped with 2 mol% Ni nanoparticles via high-pressure ball milling. Under 100 bar of hydrogen at 300 °C, these composites achieved 5.3 wt% hydrogen absorption within 5 min and completed hydrogen desorption within only 4 min at 50 mbar, demonstrating outstanding sorption kinetics.

Metal Oxide Catalysts

Compared with traditional metal-alloy catalysts, metal oxides offer superior thermal stability, better particle dispersion, and cost-effective synthesis—making them well suited to MgH_2-based hydrogen storage. The metal oxide catalysts involved in this article are shown in Table S2.

Using TiO_2 as an early model system, accumulating evidence shows that metal oxide activity depends strongly on crystal structure and morphology. Pereira et al. [28] tailored TiO_2 nanocatalysts (NR550/NR650/NR750) by calcining titanate nanotubes at 550/650/750 °C. Among them, NR750 contains a small amount of rutile. Under identical Sieverts conditions (350 °C; 10 bar H_2 absorption/0.1 bar desorption), NR750-doped MgH_2 reached 72% of its maximum absorption within 5 min, outperforming NR550 and NR650. In desorption, all samples desorbed 90% to 100% H_2 in 3 min, with NR750 hitting this benchmark earliest. Rutile TiO_2 is highly lattice-compatible with β-MgH_2 and can form a tight MgH_2–TiO_2 interface, enabling more efficient interfacial hydrogen exchange. Moreover, Ma et al. [29] synthesized TiO_2 nanosheets (TF10/TF30/TF50/TF70) with tunable 001 facet exposure via a hydrothermal method. Wulff estimates give 001 fractions of 20/34/59/88%. At 5 wt% TiO_2, the 001-rich TF70 showed the fastest kinetics, achieving 5.3 wt% hydrogen absorption in 44 s at 200 °C and 6.4 wt% hydrogen desorption in 700 s at 300 °C. The dehydrogenation onset

decreased to about 220 °C and the apparent activation energy decreased to 76 kJ mol^{-1}. Mechanistically, the major 001 facets fully expose the pentacoordinated Ti and have higher surface energy than 101, providing more active sites for H_2 dissociation/recombination.

On the basis of morphology control, methods such as single-atom anchoring and heterogeneous element doping can further reshape the interface energy band and the electronic structure of the active site to obtain better catalytic effects. Zhang et al. [30] synthesized a TiO_2-supported SAC ($Ni_{0.034}$@TiO_2) via a molten salt approach. This catalyst markedly lowered MgH_2's initial hydrogen desorption temperature to 200 °C, achieving hydrogen desorption of 4.6 wt% within 5 min at 300 °C (Fig. 3C). Notably, rapid hydrogen absorption of 6.53 wt% occurred within 10 s (Fig. 3B). Kinetic analysis indicated a substantial decrease in activation energies to 64.35 kJ/mol for desorption and 35.17 kJ/mol for hydrogen absorption. Moreover, the catalyst exhibited excellent cycling stability, retaining 97.26% hydrogen capacity after 100 cycles. These improvements were attributed to synergistic effects from atomically dispersed Ni, abundant oxygen vacancies, and multivalent Ti species, collectively facilitating electron transfer and reducing Mg–H bond strength, thereby enhancing sorption kinetics. The single-atom dispersion also maximized atom utilization and thermal stability (Fig. 3A). Moreover, Wang et al. [31] investigated nitrogen-doped Nb_2O_5, demonstrating full hydrogenation at 70 °C under 50 atm hydrogen pressure and rapid hydrogen absorption of 5.1 wt% at 100 °C within 3 min. The improved performance resulted from cooperative effects among Nb–N–O clusters, promoting hydrogen diffusion and Mg–H bond cleavage.

Compared with single-cation oxides, polymetallic oxides can further regulate hydrogen adsorption, enrich oxygen vacancies, and shorten diffusion paths by generating heterogeneous interfaces and complementary redox pairs. Liang et al. [32] synthesized NiV_2O_6 using a simple hydrothermal process, showing that MgH_2 doped with 10 wt% NiV_2O_6 substantially improved hydrogen sorption performance at 150 °C, absorbing 5.59 wt% hydrogen in 50 min. In addition, NiV_2O_6 reduced the hydrogen desorption

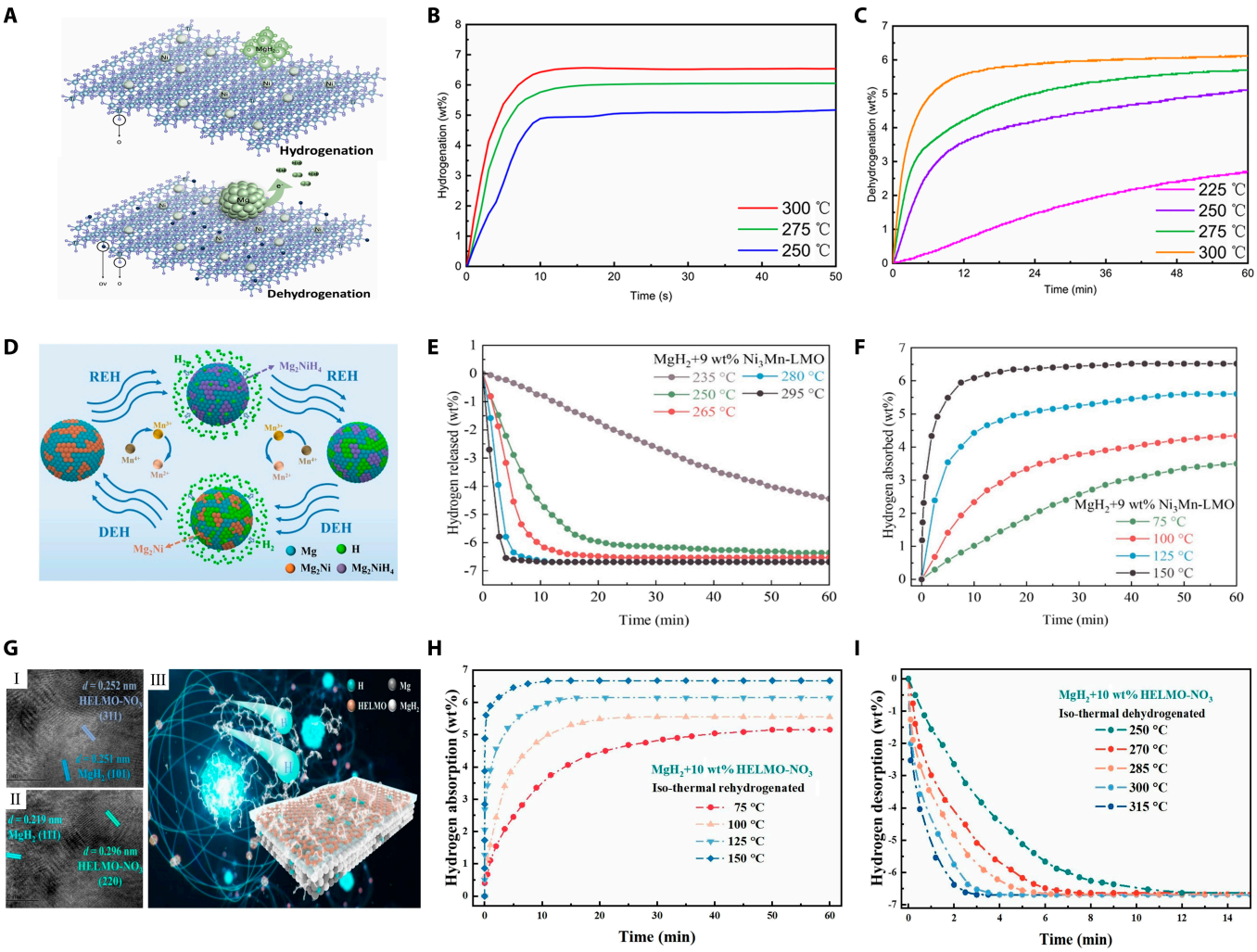


Fig. 3. (A) Schematics of the hydrogenation and dehydrogenation mechanisms of MgH_2 doped with $Ni_{0.034}$@TiO_2. (B) Hydrogenation profiles and (C) corresponding dehydrogenation profiles of MgH_2 doped with 15 wt% $Ni_{0.034}$@TiO_2 catalyst at different temperatures [30]. Reproduced with permission [30]. Copyright 2025, American Chemical Society. (D) Schematics of the hydrogenation and dehydrogenation mechanisms of MgH_2 doped with Ni_3Mn-LMO. (E) Dehydrogenation profiles and (F) corresponding hydrogenation profiles of MgH_2 doped with 9 wt% Ni_3Mn-LMO catalyst at different temperatures [34]. (G) HRTEM images (I and II) of the ball-milled MgH_2 + 10 wt% HELMO-NO_3. (III) Schematics of the hydrogenation and dehydrogenation mechanisms of MgH_2 doped with HELMO-NO_3. (H) Hydrogenation profiles and (I) corresponding dehydrogenation profiles of MgH_2 doped with 10 wt% HELMO-NO_3 catalyst at different temperatures [35].

activation energy from 119.2 to 92.9 kJ/mol, allowing 5.2 wt% hydrogen to be rapidly desorbed within 10 min at 300 °C. To further improve the catalytic performance, Zhang et al. [33] loaded the bimetallic oxide $CoMoO_4$ on rGO (reduced graphene oxide). Experiments showed that MgH_2 with the addition of 10 wt% $CoMoO_4$/rGO could absorb 4.2 wt% of hydrogen within 20 min at 150 °C and desorbed 6.25 wt% of hydrogen within 10 min at 300 °C. rGO incorporation stabilized the nanostructure and increased exposed active sites, facilitating hydrogen diffusion and reducing Mg–H bond strengths, thereby optimizing storage kinetics.

Recent studies have shown a growing trend toward 2-dimensional layered multimetal oxide catalysts, especially those with synergistic effects of cations and anions. Zhong et al. [34] synthesized 2-dimensional Ni_3Mn-based layered metal oxide (Ni_3Mn–LMO) catalysts through hydrothermal synthesis and annealing. MgH_2 composites doped with 9 wt% Ni_3Mn–LMO showed markedly reduced hydrogen desorption temperatures (190 °C) and activation energies (86.9 kJ/mol). This system desorbed 6.59 wt% hydrogen within 5 min at 295 °C (Fig. 3E) and rapidly absorbed hydrogen (6.1 wt% within 600 s at 150 °C, and 3.49 wt% within 60 min at 75 °C) (Fig. 3F). Enhanced performance resulted from the formation of Mg_2Ni/Mg_2NiH_4 phases and electron transfer facilitated by multivalent Mn species (Fig. 3D). The layered nanosheet structures also contributed high surface areas and abundant catalytic sites. Further innovation was reported by Wang et al. [35], who synthesized 2-dimensional HELMO-NO_3 catalysts via hydrothermal processing of Cr, Mn, Fe, Co, and Ni nitrates, followed by calcination at 500 °C under argon. With 10 wt% HELMO-NO_3 doping, MgH_2 exhibited a lower onset desorption temperature of 184.1 °C, desorbed 6.68 wt% hydrogen in 3 min at 315 °C (Fig. 3I), and achieved a hydrogen absorption of 5.15 wt% within 50 min at 75 °C (Fig. 3H). The exceptional performance arose from a combination of high-entropy effects, lattice distortion, multielement catalytic synergy, and an ultrathin layered structure providing ample surface areas, active sites, and diffusion channels (Fig. 3G). However, the synthesis process of this type of catalyst is complex and highly sensitive to process fluctuations, which limits its large-scale application.

Metal Halide Catalysts

Unlike metal oxides, halide catalysts (e.g., $CeCl_3$ and K_2NbF_7) exhibit strong Lewis acidity, enabling them to directly weaken the Mg–H bond strength. Additionally, these halides often react with MgH_2 to generate in situ nanophases (e.g., MgF_2 and $KMgH_3$). These phases shorten hydrogen diffusion paths and enhance storage kinetics. The metal halide catalysts involved in this article are shown in Table S3.

Metal chloride is one of the earliest and most widely used catalysts of this type, with low cost, wide source, and mature technology. In the field of transition metals, Ismail [36] investigated $HfCl_4$ doping, reporting a notable decrease in initial hydrogen desorption temperature to 265 °C, accompanied by a considerable drop in activation energy from 167 to 102 kJ/mol, thus markedly accelerating hydrogen desorption. Similarly, Suárez-Alcántara et al. [37] explored Mg–15 wt% VCl_3 composites and achieved a hydrogenation onset temperature as low as 50 °C, with an activation barrier of 63.8 kJ/mol. This composite absorbed 5 wt% hydrogen within just 1 min at 300 °C, maintaining a stable 6 wt% capacity after cycling. These advancements were mainly attributed to the refined Mg structure produced by cryo-ball milling and uniform VCl_3 dispersion, which collectively improved hydrogen diffusion and interfaces. In the field of rare earth metals, Ismail [38] observed that $LaCl_3$ doping led to a Mg_3La alloy, markedly lowering the activation energy for dehydrogenation from 166 to 143 kJ/mol. The resulting composite rapidly absorbed 5.1 wt% hydrogen within 2 min at 300 °C, surpassing pure MgH_2 (3.8 wt%). Subsequently, the group demonstrated that $CeCl_3$ promoted Ce–Mg alloy formation and $CeH_{2.73}$ during cycling, facilitating hydrogen diffusion and reducing activation energy from 167 to 149 kJ/mol. The $CeCl_3$-doped composite consequently desorbed 5.5 wt% hydrogen in 10 min at 350 °C, markedly outperforming pure MgH_2 (3.1 wt%) [39]. However, metal chlorides generate inert $MgCl_2$ during catalysis; this species accumulates on the surface and blocks diffusion and interfaces. With the accumulation of cycles, the catalytic activity will gradually decrease and the apparent activation energy will gradually increase.

Compared to chloride systems, metal fluoride catalysts exhibit stronger Lewis acidity and greater potential for interface engineering in the Mg/MgH_2 system. During reaction, in situ MgF_2 replaces the MgO passive layer, creating a fluorinated active surface and a nanoscale heterogeneous interface. This facilitates H_2 dissociation/association and interfacial diffusion. Yahya et al. [40] reported that 5 wt% K_2NbF_7 doping reduced MgH_2's hydrogen desorption activation energy from 135.3 to 96.3 kJ/mol, enabling rapid desorption of 5.2 wt% hydrogen within 5.6 min at 320 °C. Notably, this composite absorbed 4.7 wt% hydrogen in 30 min at 150 °C, markedly superior to ball-milled MgH_2 (0.7 wt%). Yan et al. [41] synthesized K_2TaF_7, demonstrating full hydrogen desorption (7.33 wt%) at 290 °C in 50 min (Fig. 4C). At 190 °C, the composite rapidly absorbed 6.56 wt% hydrogen, compared to only 3.45 wt% by unmodified MgH_2 (Fig. 4B). Structural analyses identified $KMgH_3$ and $TaH_{0.8}$ phases, acting as "hydrogen pumps", enhancing hydrogen transfer during cycling (Fig. 4A). Additionally, Yusnizam et al. [42] explored $BaCoF_4$ as an innovative catalyst. MgH_2 doped with $BaCoF_4$ showed markedly decreased hydrogen desorption onset temperature (265 °C), rapidly releasing 5.0 wt% hydrogen in 30 min at 300 °C—far exceeding undoped MgH_2 (0.1 wt%). The composite also rapidly absorbed 6.4 wt% hydrogen within just 5 min. The improved performance resulted from in situ generated CoF_3 and Ba-containing species, lowering activation barriers and promoting hydrogen diffusion. However, metal fluorides face practical drawbacks: poor thermal stability at high temperatures and susceptibility to deliquescence, both of which reduce catalytic activity. Furthermore, their synthesis and use rely heavily on an anhydrous environment and corrosion-resistant equipment. They are susceptible to hydrolysis upon exposure to moisture, generating highly toxic HF, substantially increasing safety and environmental protection costs.

The latest research focuses on achieving multiple synergies and functional integration in material structure design and catalytic mechanisms. By introducing nano-confinement, surface defect engineering, and porous supports, the activation and diffusion of hydrogen, as well as its reversible absorption and desorption, are further enhanced. Zhu et al. [43] combined NbF_5 with pBN (porous boron nitride), leveraging nano-confinement effects, greatly reducing MgH_2's hydrogen desorption temperature by 140 °C and ensuring robust cycling stability. Shi et al. [44] synthesized fluorinated TiO_2 nanosheets [TiO_{2-x}(F)] via hydrothermal methods and $NaBH_4$ reduction, introducing abundant oxygen vacancies. The resulting catalysts reduced initial hydrogen desorption

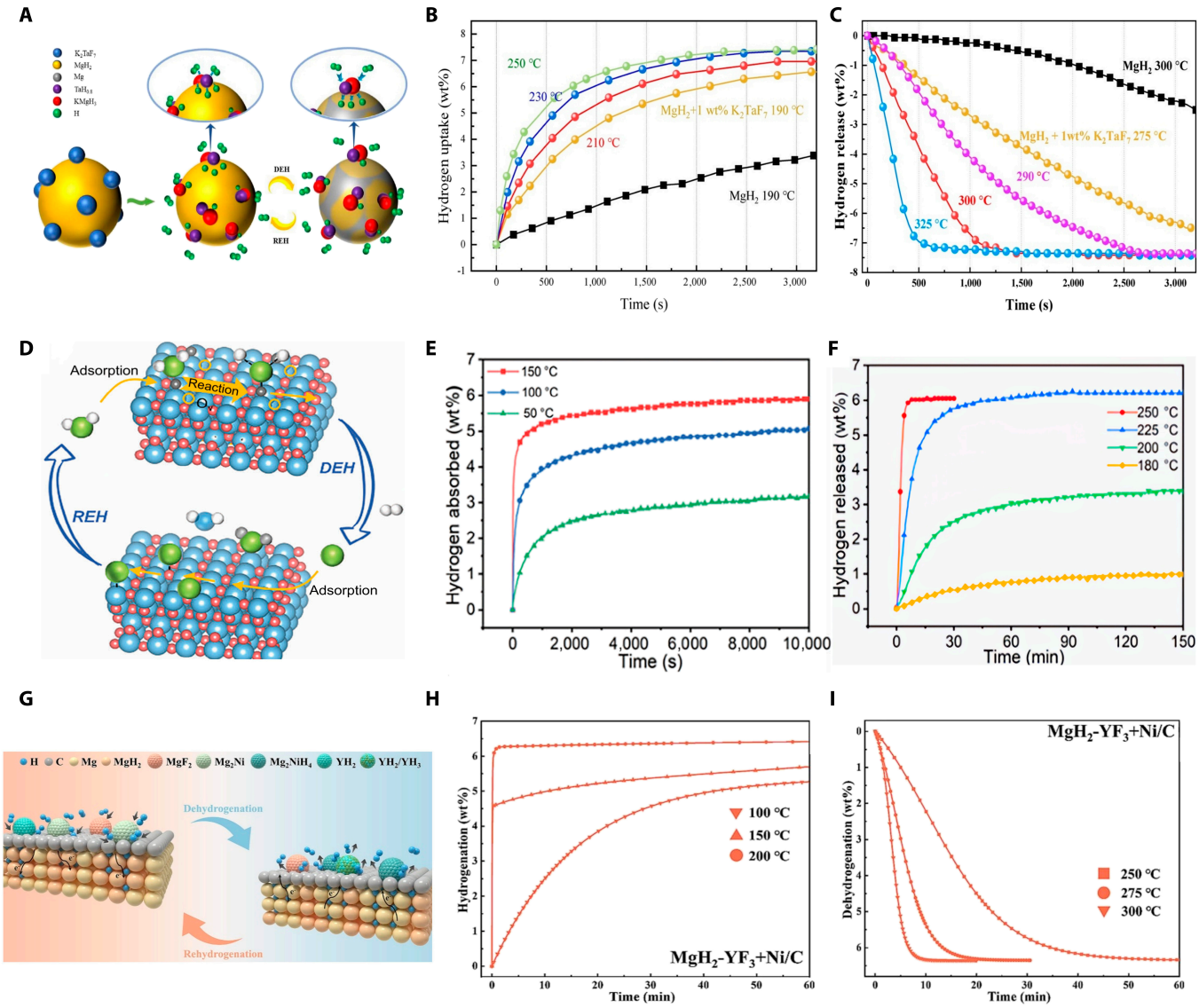


Fig. 4. (A) Schematics of the hydrogenation and dehydrogenation mechanisms of MgH_2 doped with K_2TaF_7. (B) Hydrogenation profiles and (C) corresponding dehydrogenation profiles of MgH_2 doped with 1 wt% K_2TaF_7 catalyst at different temperatures [41]. (D) Schematics of the hydrogenation and dehydrogenation mechanisms of MgH_2 doped with TiO_{2-x}(F). (E) Hydrogenation profiles and (F) corresponding dehydrogenation profiles of MgH_2 doped with TiO_{2-x}(F) catalyst at different temperatures [44]. (G) Schematics of the hydrogenation and dehydrogenation mechanisms of MgH_2 doped with YF_3 and Ni/C. (H) Hydrogenation profiles and (I) corresponding dehydrogenation profiles of MgH_2 doped with YF_3+Ni/C catalyst at different temperatures [45].

temperature to 189 °C, enabling rapid desorption of 6.0 wt% hydrogen within 6 min at 250 °C (Fig. 4F), and maintaining 93.3% capacity after 10 cycles. Additionally, the composite demonstrated superior hydrogen absorption, absorbing 6.79 wt% at 150 °C and even 3.0 wt% within 120 min at temperatures as low as 50 °C (Fig. 4E). The enhanced performance stemmed from oxygen vacancies, optimized hydrogen dissociation pathways, and reactive species (MgF_2, hydrogen-rich solid solutions) formed in situ (Fig. 4D). Recently, Zhang et al. [45] incorporated YF_3 and bio-derived porous Ni/C into MgH_2 via short-duration ball milling, forming a well-dispersed dual-catalyst composite. The MgH_2–10 wt% (YF_3+Ni/C) sample exhibited lowered initial desorption temperature (221.1 °C), releasing 5.22 wt% hydrogen in 5 min at 300 °C and 5.74 wt% within 30 min at 250 °C (Fig. 4I), with rapid reabsorption (5.93 wt%) within 15 s at 200 °C (Fig. 4H). Capacity retention reached 98.4% after 30 cycles at 300 °C. These improvements arise from reversible YH_2/YH_3 and Mg_2Ni/Mg_2NiH_4 "hydrogen-pump" mechanisms, plus abundant Ni nanoparticles dispersed in defect-rich carbon. Together, they enhance H_2 dissociation and diffusion kinetics while limiting particle growth (Fig. 4G).

Metal Sulfide Catalysts

Compared to metal halides, metal sulfide catalysts exhibit excellent resistance to hydrolysis and retain structural stability at elevated temperatures (up to 500 °C). The metal sulfide catalysts involved in this article are shown in Table S4.

The catalytic activity can be effectively improved by regulating the micromorphology of the catalyst. Layered structures can be exfoliated into 2D nanosheets with high specific surface area. This exposes many active sites and accelerates in-plane electron/ion transport, yielding higher catalytic activity. Wang et al. [3] systematically assessed various sulfides (TiS_2, NbS_2,

MoS_2, MnS, CoS_2, and CuS) as MgH_2 catalysts, identifying TiS_2 with a layered structure as particularly effective. It substantially decreased the initial hydrogen desorption temperature by 126 °C, lowering the activation barrier to 50.8 kJ/mol. In addition to structure, the control of particle size is also an effective means to improve catalytic activity. Cheng et al. [46] synthesized a MgH_2–Fe_7S_8 composite by ball milling industrial MgH_2 and 16.7 wt% nano-Fe_7S_8. At 350 °C, the composite desorbed 4.40 wt% H_2 within 30 min, markedly higher than the 2.48 wt% of pure MgH_2. Furthermore, at 200 °C and 3 MPa H_2, the composite absorbed 4.00 wt% H_2 within 30 min, surpassing the 1.85 wt% of pure Mg. Fe_7S_8 doping reduced the apparent dehydrogenation activation energy from 165.9 kJ/mol to 130.0 kJ/mol. Kinetic analysis showed a shift from interface-controlled to diffusion-controlled dehydrogenation. In situ Fe and Mg_2FeH_6 formed during cycling, promoting Mg–H bond cleavage and hydrogen diffusion.

Recent research has turned to constructing catalysts with hierarchical or composite structures to provide more reactive sites. Xie et al. [47] prepared layered walnut shell NiS@NTA by hydrothermal carbonization. Doping 5 wt% NiS@NTA with Mg resulted in the composite absorbing 3.0 wt% H_2 in 60 min at 80 °C and releasing 3.5 wt% H_2 in 60 min at 300 °C, while simultaneously lowering the onset dehydrogenation temperature to 235 °C. The composite retained 97% of its capacity after 20 cycles. This performance improvement was attributed to the carefully designed layered walnut shell microstructure, which provided abundant interfaces and catalytically active sites. This morphology facilitated the in situ formation of MgS and Mg_2Ni, thereby promoting electron transfer and hydrogen diffusion. However, morphology control alone offers limited gains; additional strategies are usually required to further boost catalytic performance.

Because different metal sites have complementary electronic structures and functions, multimetallic catalysts can, under close contact and in situ reconstruction, form mass-transfer interfaces with lower energy barriers. These interfaces deliver superadditive, synergistic interfacial catalysis. Tan et al. [48] synthesized a Mg-Ni-TiS_2 nanocomposite via a solution method, in which Mg and Ni nanoparticles were in situ reduced and highly dispersed on TiS_2 nanosheets. At 300 °C, the composite completely absorbed hydrogen within 60 s and desorbed 4.60 wt% H_2 within 240 s, markedly outperforming pure Mg. Mechanistic studies show that in situ-formed Mg_2NiH_4 and TiH_2 create fast hydrogen-diffusion pathways and lower interfacial reaction barriers. Meanwhile, MgS and TiS_2 anchor the catalytic nanoparticles and inhibit grain growth. The advancement of bimetallic sulfide catalysts has further elevated MgH_2-based storage performance. Chen et al. [49] developed $NiCo_2S_4$ doping (10 wt%), markedly lowering the onset hydrogen desorption temperature to 203 °C and achieving 6.11 wt% hydrogen desorption within 5 min at 325 °C, with activation energy decreased to 86.5 kJ/mol (Fig. 5C). Furthermore, hydrogen absorption reached 5.54 wt% within 1 min at 150 °C, greatly surpassing undoped MgH_2 (2.04 wt% within 10 min) (Fig. 5B). This enhanced performance arose from the formation of Mg_2Ni, Mg_2Co, and MgS phases, collectively facilitating hydrogen dissociation and diffusion and enabling a reversible hydrogen pumping effect (Fig. 5A). Fu et al. [7] additionally synthesized $FeNi_2S_4$, reporting that MgH_2 doped with $FeNi_2S_4$ decreased the hydrogen desorption activation energy from 79.8 to 65.5 kJ/mol, markedly boosting hydrogen cycling stability and kinetics.

Some materials with highly designable porous structures and extremely high specific surface areas, such as MOFs (metal–organic frameworks) and MXenes, can be used as sacrificial templates to prepare catalysts with excellent catalytic activity. Fu et al. [50] synthesized FeCoS@C through carbonization and sulfurization of MOF precursors. With 5 wt% doping into MgH_2, the resulting composite rapidly absorbed 6.84 wt% hydrogen within 60 min at 200 °C (Fig. 5E). Additionally, the onset desorption temperature decreased markedly to 277 °C, highlighting improved kinetics (Fig. 5F). The enhancement arises from a multiphase system—Mg_2Co, α-Fe, and Co_3Fe_7—formed by in situ decomposition of FeCoS@C. These phases facilitate hydrogen diffusion via a "hydrogen channeling" effect. Moreover, MgS formation further improved structural and catalytic stability (Fig. 5D). Zheng et al. [51] similarly prepared $FeNi_3$–S catalysts from NiFe-MOFs. MgH_2 doped with 10 wt% $FeNi_3$–S showed a decreased initial hydrogen desorption temperature (202 °C), 123 °C below pristine MgH_2, releasing 6.57 wt% hydrogen in 1,000 s versus 2.0 wt% for undoped MgH_2. This improvement was attributed to synergistic hydrogen pathways involving hydrogen pumping (Mg_2Ni/Mg_2NiH_4) and enhanced diffusion at Fe/MgS interfaces. Similarly, Yuan et al. [52] fabricated S–Ti_3C_2 via a 2-step etching and thiourea treatment (Fig. 5G). Incorporating 5 wt% S–Ti_3C_2 into MgH_2 markedly enhanced hydrogen storage, reducing the initial desorption temperature to 173 °C and enabling rapid desorption of 7.0 wt% hydrogen within 7 min at 240 °C (Fig. 5H). For hydrogen absorption, the composite absorbed 5.1 wt% hydrogen in only 68 s at 200 °C and still managed 4.7 wt% within 60 min at 50 °C (Fig. 5I). Performance enhancements were mainly due to combined sulfur doping and multivalent Ti species, forming Ti^0/Ti^{2+} active sites (Fig. 5G), promoting Mg–H bond cleavage, and improving interface stability during cycling.

Carbon-Based Composite Catalysts

Carbon-based composites have emerged as a research hotspot in the field of MgH_2 hydrogen storage catalysis. These materials integrate the high catalytic activity of traditional catalysts—such as metals and metal oxides—with the inherent advantages of carbon materials, including excellent chemical stability, high specific surface area, and good electrical conductivity. This combination substantially enhances the adsorption, dissociation, and diffusion of hydrogen molecules. Additionally, a carbon coating acts as a protective layer, suppressing particle agglomeration and sintering. As a result, it improves particle dispersion and cycling stability. Consequently, carbon-supported composites offer a compelling approach to boost both the efficiency and longevity of MgH_2-based hydrogen storage systems.

One-dimensional carbon material

One-dimensional carbon materials focus on building a continuous "transport network" for hydrogen storage reactions. They form thermally and electrically conductive percolation pathways with low thresholds. These pathways markedly alleviate thermal hysteresis and charge-transfer bottlenecks during hydrogen absorption and desorption. Furthermore, tube cavities or grooves provide linear confinement that uniformly distributes MgH_2 and promoter metals at the nanoscale. This shortens diffusion paths and inhibits aggregation and particle growth. Relevant one-dimensional carbon-based catalysts studied herein are summarized in Table S5.

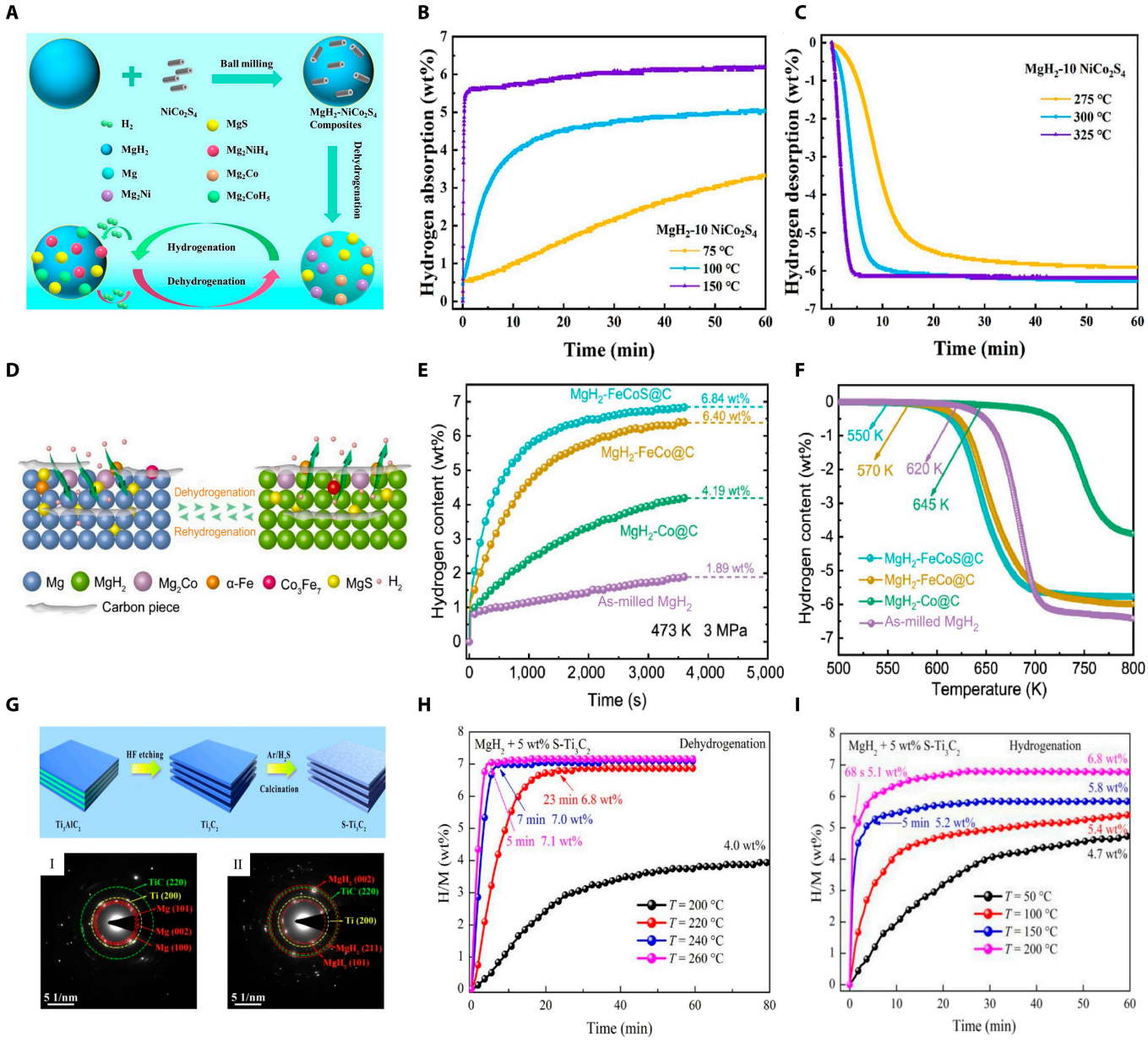


Fig. 5. (A) Schematics of the hydrogenation and dehydrogenation mechanisms of MgH_2 doped with $NiCo_2S_4$. (B) Hydrogenation profiles and (C) corresponding dehydrogenation profiles of MgH_2 doped with 10 wt% $NiCo_2S_4$ at different temperatures [49]. (D) Schematics of the hydrogenation and dehydrogenation mechanisms of MgH_2 doped with FeCoS@C. (E) Hydrogenation profiles of MgH_2 doped with catalysts of different components at 3 MPa and 473 K. (F) TPD curves of the MgH_2 doped with catalysts of different components [50]. (G) Synthesis scheme of S-Ti_3C_2 and selected-area electron diffraction (SAED) patterns for hydrogenated (I) and dehydrogenated (II) MgH_2 containing 5 wt% S- Ti_3C_2. (H) Hydrogenation profiles and (I) corresponding dehydrogenation profiles of MgH_2 doped with 5 wt% S-Ti_3C_2 catalyst at different temperatures [52].

CNTs (carbon nanotubes), with their dual-channel structure of a hollow lumen and outer wall, combine efficient hydrogen diffusion with confinement. Compared to other one-dimensional carbon materials, CNTs' continuous inner lumen and more controllable conductive network offer advantages in low-temperature dynamics and cycle life. Liu et al. [53] synthesized BCNTs (bamboo-shaped CNTs) encapsulating MgH_2, achieving rapid hydrogen absorption of 5.79 wt% within 5 min at 250 °C by restricting MgH_2 particle sizes to 15 to 20 nm. The activation energy for hydrogen desorption was markedly decreased from 209.18 to 97.94 kJ/mol, indicating that BCNTs are highly effective for high-density hydrogen storage. Duan et al. [54] prepared Ni-CNTs via hydrothermal and calcination. MgH_2 with 5 wt% Ni-CNT addition desorbed 7.29 wt% H_2 within 60 min at 250 °C, reducing the apparent dehydrogenation activation energy to 74.8 kJ mol^{-1}. Furthermore, 7.2 wt% H_2 was rapidly adsorbed within 30 min at 200 °C. Meanwhile, the capacity of approximately 7.2 wt% was maintained over 10 cycles. This enhanced performance stems from the nanoconfinement effect of the CNTs and the catalytic activity of interfacial Ni (10 to 12 nm metallic Ni nanoparticles uniformly dispersed on 30 nm CNTs), which effectively promotes the dissociation/recombination and diffusion of H_2.

Through interface engineering, a CNT-based multicomponent system can establish a cascade pathway—dissociation → spillover → diffusion → hydrogen pump—and a stable confined

microenvironment. This combination lowers the initial desorption temperature and apparent activation energy, and it markedly improves cycle stability and rate performance. Lu et al. [55] synthesized a composite catalyst comprising TiO_2–$ZnTiO_3$ on CNTs, which reduced the initial hydrogen desorption temperature from 345 to 197 °C and decreased the activation energy by 42 kJ/mol. The resulting composite delivered 6.1 wt% H_2 in 10 min at 300 °C, with 97% capacity retention after 20 cycles. The enhanced performance resulted from the cooperative interaction of CNTs and the formation of active phases such as TiO_2, $MgTi_2O_4$, and Zn_4TiO_6. Fu et al. [56] fabricated NiFe@CNT catalysts, which effectively decreased the initial MgH_2 desorption temperature to 225 °C and lowered the activation energy to 49.7 kJ/mol. This performance improvement originated from the combined hydrogen pump function of Mg_2Ni/Mg_2NiH_4 and hydrogen diffusion channels from α-Fe. Wan et al. [57] developed a VTiFe-CNTs dual-phase catalyst, lowering the dehydrogenation temperature of MgH_2 to 200 °C and facilitating rapid hydrogen desorption of 6.3 wt% in 5 min, with 97.3% capacity retention upon cycling. The improvement was linked to abundant active catalytic sites formed by α-Fe and FCC phases, as well as the confinement effects of CNT structures. Similarly, Duan et al. [58] synthesized a bimetallic Co@Pd-CNT catalyst, achieving rapid hydrogen desorption of 7.30 wt% in 8 min at 325 °C, without noticeable performance decay after 10 cycles. This superior catalytic activity was due to dual-catalytic mechanisms involving hydrogen pumping and spillover effects. However, the relatively high price of CNTs severely limits their practical application.

One-dimensional carbon materials prepared by MOF derivatization are relatively low in cost and can achieve a certain balance between performance and cost, making them a research hotspot in recent years. Ren et al. [59] fabricated MgH_2/Ni@pCNF composites by supporting Ni nanoparticles on MOF-derived N-doped pCNFs (porous carbon nanofibers). The composites demonstrated a reduced activation energy of 96.58 kJ/mol for hydrogen desorption, a lower initial desorption temperature of 200 °C, and retained 95.4% capacity after 10 cycles at 300 °C. Hu et al. [60] synthesized TM/C catalysts (TM = Fe, Ni) using MOF-derived porous carbon (Fig. 6A). MgH_2 modified with 10 wt% TM/C exhibited a markedly lowered initial hydrogen desorption temperature of 194 °C, with a reduced activation energy of 77.3 kJ/mol, releasing approximately 6.5 wt% H_2 below 300 °C (Fig. 6B). Then, the composite achieved rapid absorption of 6.2 wt% within 60 s at 150 °C and 5.7 wt% within 60 min at 100 °C (Fig. 6C). These enhancements were driven by the combined catalytic activities of Fe and Ni: Fe facilitated hydrogen dissociation, whereas Ni enhanced the reversible formation of Mg_2Ni/Mg_2NiH_4 phases, resulting in effective hydrogen transport. Additionally, the carbon matrix structure prevented particle agglomeration and provided pathways for hydrogen diffusion (Fig. 6A).

Two-dimensional carbon materials

Two-dimensional carbon materials focus on the construction and regulation of "interfaces and sites". Their ultra-high surface area and wrinkled structure provide uniform and secure anchoring for nanocatalytic particles. Their "thin blanket" coating and planar confinement enable high-density active interfaces even at low loadings. The abundant vacancy defects also create designable chemically active sites [61]. The 2-dimensional carbon material catalysts involved in this article are shown in Table S6.

Gr (Graphene)-based carbon-based catalysts are the most common 2-dimensional carbon materials. They rely on ultra-high specific surface area and rich defects and functional groups to form a "multiactive site, high conductivity" platform, which can coordinate the adsorption and dissociation of hydrogen molecules, sheet confinement, and electron/heat transport. At the same time, their continuous π conjugation gives them more advantages in low-temperature kinetics and cyclic stability. Verma et al. [62] investigated TiH_2@Gr catalysts and reported that the synergistic interaction with MgH_2 decreased the initial hydrogen desorption temperature to 204 °C and markedly reduced the activation barrier, effectively promoting hydrogen desorption kinetics. Subsequently, Song et al. [63] prepared FeOOH nanodots anchored onto graphene (FeOOH NDs@Gr), enabling the composite to store 6.0 wt% hydrogen at 200 °C under a pressure of 3.2 MPa within 60 min, maintaining 98.5% capacity retention after 20 cycles. To further enhance catalytic activity, Huang et al. [61] developed a Gn (graphene nanosheets)-supported bimetallic oxide catalyst Sc_2O_3/TiO_2@Gn. When 10 wt% Sc_2O_3/TiO_2@Gn was incorporated into MgH_2, the composite showed markedly improved hydrogen absorption kinetics, absorbing 6.55 wt% hydrogen within 1 min at 300 °C and desorbing 5.71 wt% within 10 min. Moreover, the initial dehydrogenation temperature decreased to 140 °C. The composite exhibited superior cycling stability, maintaining 99.1% hydrogen storage capacity after 50 cycles. This enhanced performance was linked to the cooperative catalytic activity of Sc_2O_3 and TiO_2, the presence of oxygen vacancies, and graphene's role in preventing Mg particle agglomeration and catalyst dispersion. On this basis, Guemou et al. [64] designed a ternary Ni-Nb/rGO catalyst, demonstrating that doping MgH_2 with 10 wt% Ni–Nb/rGO markedly decreased the activation energy to 57.8 kJ/mol. This composite absorbed 2.75 wt% hydrogen in 30 min at 75 °C under 3 MPa (Fig. 6E) and achieved 5.9 wt% hydrogen desorption in 10 min at 260 °C, with a maximum desorption of 6.41 wt% within just 5 min at 300 °C (Fig. 6F). This performance confirmed excellent hydrogen storage properties at moderate temperatures. Mechanistic studies indicated uniform dispersion of $Ni/NiO/Nb_2O_5$ nanoparticles on rGO sheets formed through ball milling, which improved dispersion and prevented agglomeration. During cycling, the Ni and Nb-based phases promoted hydrogen desorption, while rGO enhanced conductivity and stabilized catalyst dispersion (Fig. 6D).

MXenes are a class of 2-dimensional transition metal carbide/nitride/carbonitride flakes derived from a MAX phase by selectively removing the A layer. Leveraging a transition metal-containing layered carbon/nitride framework and programmable surface terminations (–O, –OH, –F), MXenes offer advantages in interfacial electronic structure control and active site construction. Li et al. [65] studied Ti_2C MXene, demonstrating that multivalent Ti atoms promoted electron transfer processes between H^- and Mg^{2+}, reducing the activation energy for hydrogen desorption from 107.3 to 71.7 kJ/mol, and lowering the onset temperature by 37 °C (from 327 to 290 °C). Liu et al. [66] developed a dual-MXene catalytic system of V_2C and Ti_3C_2, which reduced the initial dehydrogenation temperature of MgH_2 to 180 °C, achieving 5.1 wt% hydrogen desorption within 60 min at 225 °C, revealing synergistic interactions between the 2 MXene phases. Lu et al. [67] explored Nb_2CT_x MXene codoped with N/S elements, effectively lowering the hydrogen diffusion barrier, enabling hydrogen desorption of 4.78 wt% within 30 min at 225 °C, with overall enhanced storage performance. In recent research, Zhu et al. [68] fabricated

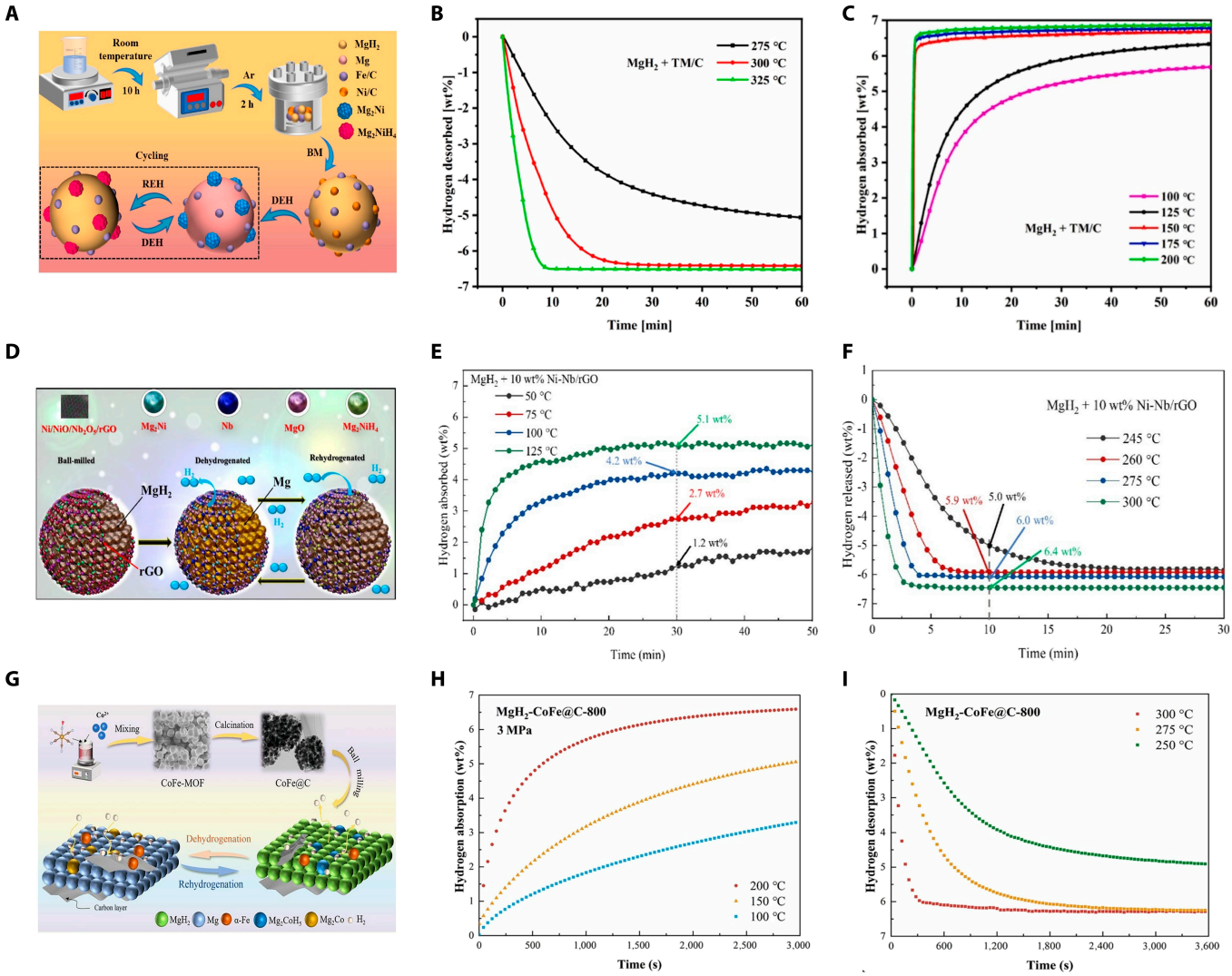


Fig. 6. (A) Schematics of the hydrogenation and dehydrogenation mechanisms of MgH_2 doped with TM/C. (B) Dehydrogenation profiles and (C) corresponding hydrogenation profiles of MgH_2 doped with TM/C catalyst at different temperatures [60]. (D) Schematics of the hydrogenation and dehydrogenation mechanisms of MgH_2 doped with Ni-Nb/rGO. (E) Hydrogenation profiles and (F) corresponding dehydrogenation profiles of MgH_2 doped with 10 wt% Ni-Nb/rGO catalyst at different temperatures [64]. (G) Schematics of the hydrogenation and dehydrogenation mechanisms of MgH_2 doped with CoFe@C-800. (H) Hydrogenation profiles and (I) corresponding dehydrogenation profiles of MgH_2 doped with 10 wt% CoFe@C-800 catalyst at different temperatures [76].

an In@Ti-MX nanocomposite, composed of ultradispersed indium nanoparticles anchored onto single/few-layered Ti_3C_2 MXene nanosheets. By incorporating 15 wt% In@Ti-MX into MgH_2, the composite absorbed 4.9 wt% hydrogen at 200 °C and desorbed 5.25 wt% hydrogen within 10 min at 325 °C, with reduced hydrogen desorption activation energy of 95.2 kJ/mol. Furthermore, the reaction enthalpy decreased to −66.2 kJ/mol, substantially improving thermodynamics. This performance arises from synergy between Ti_3C_2 MXene sheets and In/TiH_2 phases, which catalyze H_2 dissociation/recombination and provide diffusion pathways, thereby weakening Mg–H bonds. The disadvantages of using MXene as a carbon-based support are also notable. MXene requires the preparation of a MAX precursor, followed by etching, exfoliation, end group and oxidation control, and repeated cleaning and dispersion steps. This requires higher yield and stability management. While the cost of MXene is decreasing with the advancement of HF-free and continuous processes, it currently remains substantially higher than mainstream graphene.

Using MOF as a precursor for pyrolysis, flaky porous carbon nanosheets can be obtained in a directed manner. The thickness, pore size/specific surface area, heteroatom doping, and in situ anchoring of metal nanoparticles (or their oxides/carbides) can be designed by selecting layered/flaky MOFs, adjusting nitrogen-containing ligands and metal nodes, and controlling temperature and atmosphere. Lan et al. [69] prepared MOF-derived CN (carbon nitride) nanosheets. These nanosheets were codoped with disc-shaped Ni and TiO_2 nanoparticles, and the composite was denoted as (Ni, TiO_2)CN. Doping 10 wt% (Ni, TiO_2)CN into MgH_2 enabled rapid desorption, reaching 5.94 wt% H_2 within 5 min at 300 °C. This also lowered the onset of dehydrogenation to 204 °C and the activation energy from 152.1 to 83.1 kJ mol^{-1}. This also facilitated rapid hydrogen absorption, reaching 6.17 wt% within 10 min at 125 °C. Furthermore, the composite exhibited excellent cycling stability, retaining approximately 6.40 wt% H_2 after 100 cycles. The performance improvement is attributed to the in situ formed Mg_2Ni/Mg_2NiH_4 (acting as a "hydrogen pump"), redox-active Ti species that promote charge transfer, and

N-doped carbon nanosheets that suppress particle agglomeration and disperse the active material.

Three-dimensional carbon materials

Three-dimensional carbon materials focus on "bulk confinement and macroscopic formation". Their hierarchical pores offer a large interfacial area and ample channels for hydrogen storage and desorption. They also maintain interparticle connectivity and efficient gas diffusion. The 3-dimensional carbon material catalysts involved in this article are shown in Table S7.

Carbon spheres are one of the most common 3-dimensional carbon materials. They can evenly and firmly anchor nanocatalytic particles on their surfaces and within their pores, providing pathways for rapid electron and heat transfer. Their spherical structure also acts as a buffer and "solid lubricant" during circulation. Their mature synthesis route, low equipment requirements, and undemanding raw material purity make them relatively scalable. Wang et al. [70] explored Ni@NCS (Ni-coated nitrogen-doped carbon spheres), which exhibited a hydrogen absorption capacity of 4.2 wt% at 100 °C within 60 min. Notably, the onset desorption temperature dropped to 246 °C—substantially lower than that of pure MgH_2. Such improvement was attributed to reversible Mg_2NiH_4/Mg_2Ni transformation (hydrogen pump effect), nitrogen-doping-induced active sites, and enhanced electron transfer, forming a triple-synergistic mechanism for improved hydrogen kinetics and cycling. Then, Wang et al. [71] prepared Ni@PHCNSs (porous hollow carbon nanospheres) loaded with uniformly dispersed Ni nanoparticles. This MgH_2 composite exhibited a lowered initial hydrogen desorption temperature of 190 °C and maintained 94.1% hydrogen capacity after 50 cycles, confirming excellent cycling durability. Similarly, Soni et al. [72] studied Fe-HCS (Fe-loaded hollow carbon spheres), achieving a reduced desorption onset temperature of 225.9 °C and lowering activation energies for hydrogen absorption and desorption to 84.9 kJ/mol. The material also displayed outstanding stability over 24 cycles.

Other 3-dimensional carbon materials, including CMK-3 (mesoporous carbon), amorphous carbon, and graphene nanorods, have also exhibited promising catalytic activities. Cheng et al. [73] studied $Pd_{30}Ni_{70}$ supported on CMK-3, observing reduced hydrogenation and dehydrogenation activation energies of 65.9 and 78.9 kJ/mol, respectively. This composite achieved 4.0 wt% hydrogen absorption in 18,000 s at 100 °C, indicating notable low-temperature hydrogen storage performance. Yu et al. [74] found that amorphous carbon formed in situ reduced activation energy for hydrogen desorption to 87.2 kJ/mol, allowing MgH_2 to absorb 5.62 wt% hydrogen within 3,600 s at 150 °C. Zhou et al. [75] developed an Fe–Ni alloy-decorated 3D graphene (Fe–Ni@3DG) catalyst. The resulting MgH_2 composite exhibited hydrogen absorption of 6.35 wt% in just 100 s, and hydrogen desorption of 5.13 wt% in 500 s at 300 °C under 50 atm hydrogen pressure, maintaining excellent reversibility after 7 cycles. Notably, the ball-milled 3-dimensional graphene structure developed cracks and pores, markedly enhancing hydrogen diffusion pathways and interfacial catalytic activity. However, the cost of these carbon materials is generally high, limiting their widespread application.

The targeted design of 3-dimensional carbon-supported catalysts with multiple catalytic functions through the adjustable nanostructure of MOF materials is currently a popular research direction. Hu et al. [60] investigated Fe/C and Ni/C catalysts derived from MOFs. The MgH_2–Fe/Ni/C composite showed reduced initial desorption temperature at 194 °C and hydrogen absorption of 6.2 wt% within 60 s at 150 °C. Similarly, Li et al. [76] fabricated flower-like CoFe@C catalysts via thermal decomposition of CoFe-based MOF precursors under nitrogen (Fig. 6G). These catalysts demonstrated excellent catalytic efficiency for MgH_2-based hydrogen storage. The composite exhibited rapid hydrogen absorption, achieving a capacity above 6 wt% within 2,000 s at 200 °C and 3 MPa (Fig. 6H). Additionally, it desorbed 6.0 wt% hydrogen within 400 s at 300 °C, markedly outperforming pristine MgH_2 (Fig. 6I). Notably, the CoFe@C catalyst lowered the activation energy for hydrogen desorption by 38%, decreased the onset desorption temperature to 175.9 °C, and retained reversible storage capacity of 6.1 wt% after 20 cycles, indicating superior cycle stability. Mechanistic analysis confirmed that improved catalytic performance resulted from synergistic interactions among α-Fe, Mg_2CoH_5, and Mg_2Co phases generated in situ, in combination with conductive carbon matrices that facilitated hydrogen dissociation and diffusion without compromising catalyst integrity (Fig. 6G). Guo et al. [77] further demonstrated that Ni–MOF-derived carbon-supported Mg–Mg_2Ni composites decreased activation energy to 77.6 kJ/mol, retaining 6.0 wt% hydrogen after 10 cycles, validating the effectiveness of MOF-derived carbon nanostructures in enhancing hydrogen storage kinetics of MgH_2.

Other Compound Catalysts

Catalysts such as metal nitrides, carbides, borides, and MOFs have shown remarkable capability in promoting MgH_2-based hydrogen storage performance. These materials effectively lower hydrogen desorption temperatures, enhance hydrogen diffusion kinetics, and improve cycle durability. Other types of catalysts involved in this article are shown in Table S8.

Metal nitrides combine high activity and durability. The strong hybridization of lattice nitrogen with transition metals shifts the metal's d-band downward and narrows it, placing hydrogen adsorption within the Sabatier optimal range. Simultaneously, the metal (Lewis acid) and adjacent nitrogen (Lewis base) sites heterolytically split H_2 into M–H and N–H. The resulting hydrogen spillover rapidly transports H and markedly lowers the barrier for Mg–H bond cleavage and recombination. Sun et al. [78] synthesized Ni/Mo_2N catalysts via a hydrothermal approach. After doping into MgH_2, the initial dehydrogenation temperature dropped to 186.3 °C, about 135.8 °C below pure MgH_2. The catalyst markedly enhanced hydrogen storage kinetics, allowing the desorption of 6.80 wt% hydrogen within 5 min at 325 °C and 6.09 wt% within 10 min at 285 °C (Fig. 7C). Additionally, the composite absorbed 5.46 wt% hydrogen in 15 min at 125 °C, demonstrating substantial improvement over pristine MgH_2 (Fig. 7B). Structural characterization confirmed that Ni/Mo_2N promoted reversible Mg_2Ni/Mg_2NiH_4 formation and introduced stable active sites for rapid hydrogen diffusion pathways (Fig. 7A). Wu et al. [79] synthesized Ni/VN catalysts through solvothermal techniques. MgH_2 doped with 7 wt% Ni/VN exhibited a lower onset hydrogen desorption temperature of 205 °C, approximately 168 °C lower compared with pure MgH_2 (373 °C), releasing 6.4 wt% hydrogen within 3 min at 325 °C and 5.6 wt% within 1 h at 240 °C (Fig. 7E). It also absorbed 6.0 wt% hydrogen within 5 min at 150 °C, maintaining a capacity retention of 91.6% after 10 cycles at 300 °C (Fig. 7F). XRD (x-ray diffraction) analyses confirmed the generation of Mg_2Ni/Mg_2NiH_4 phases, and XPS (x-ray photoelectron spectroscopy) revealed uniformly dispersed Ni nanoparticles. The VN component provided stable active sites and enhanced hydrogen diffusion, synergistically improving the hydrogen storage efficiency (Fig. 7D).

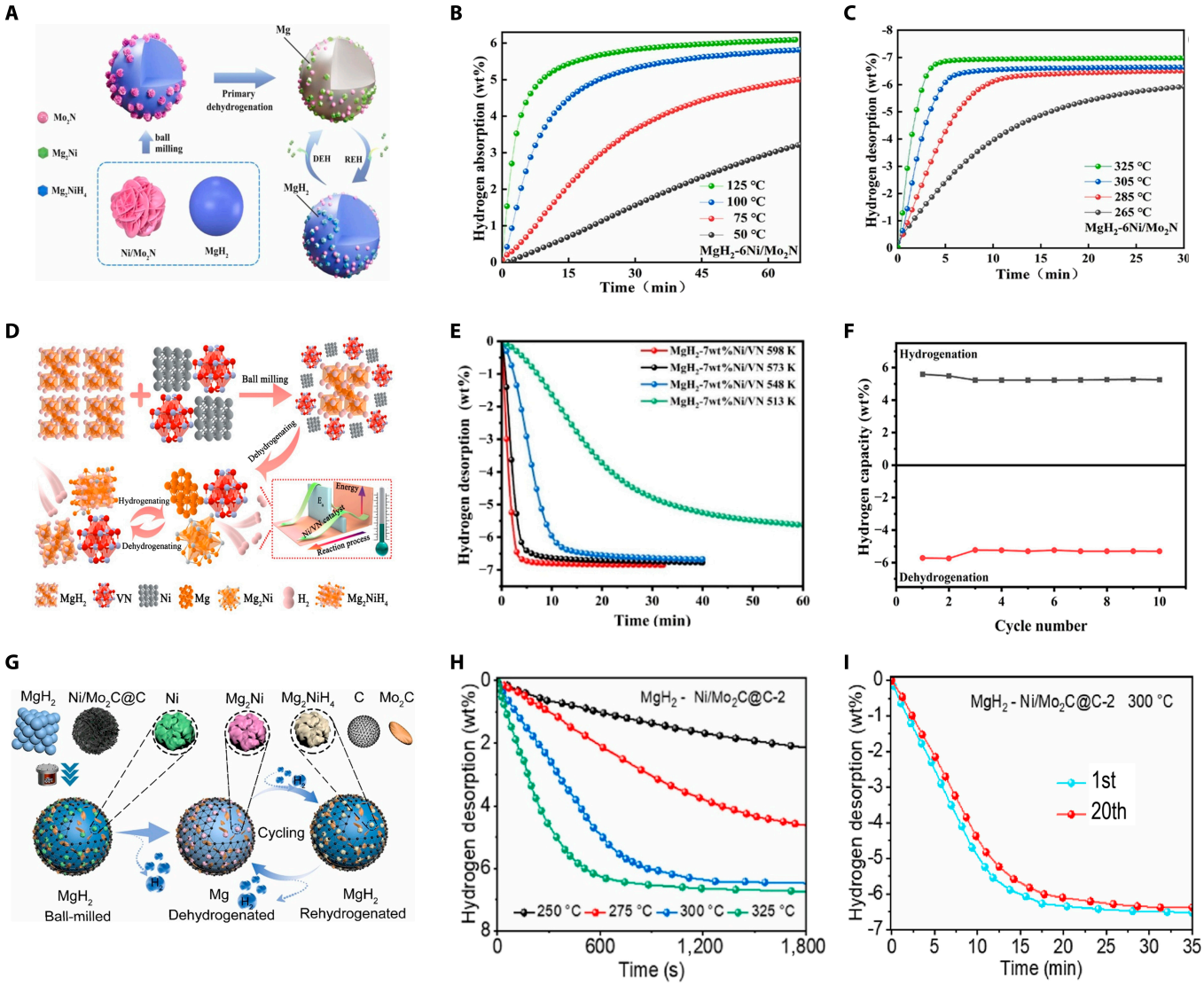


Fig. 7. (A) Schematics of the hydrogenation and dehydrogenation mechanisms of MgH_2 doped with Ni/Mo_2N. (B) Hydrogenation profiles and (C) corresponding dehydrogenation profiles of MgH_2 doped with Ni/Mo_2N catalyst at different temperatures [78]. (D) Schematics of the hydrogenation and dehydrogenation mechanisms of MgH_2 doped with Ni/VN. (E) Dehydrogenation behavior of MgH_2 doped with 7 wt% of Ni/VN at different temperatures. (F) Cycling behavior of MgH_2 with 7 wt% Ni/VN at 573 K [79]. (G) Schematics of the hydrogenation and dehydrogenation mechanisms of MgH_2 doped with Ni/Mo_2C@C-2. (H) Dehydrogenation behavior of MgH_2 doped with 7.5 wt% Ni/Mo_2C@C-2 at different temperatures. (I) Cycling behavior of MgH_2 with 7.5 wt% Ni/Mo_2C@C-2 at 300 °C [81].

Metal carbides similarly utilize p–d hybridization with nonmetallic (C) atoms to shift the metal's d-band downward, placing hydrogen adsorption within the Sabatier optimum. This heterolytic H_2 synergistically splits H_2 between metal and nonmetallic sites, promoting hydrogen diffusion. However, nitrogen's higher electronegativity enhances hydrogen pumping capacity, while carbon exhibits stronger covalent interactions with metals, resulting in improved electron transport and sintering resistance. Yao et al. [80] investigated the synergistic role of transition metal carbides (TiC, ZrC, and WC) combined with Mg_2NiH_4, identifying TiC as most effective. The MgH_2–TiC composite showed a hydrogen desorption onset at 216 °C and retained 95% hydrogen storage capacity after 10 cycles. The cooperative effects between Mg_2NiH_4 and TMCs enhanced kinetics by facilitating electron transfer, markedly reducing activation energies. Yuan et al. [81] fabricated Ni/Mo_2C@C catalysts by pyrolysis of polydopamine-coated $NiMoO_4$ precursors. The resulting composite displayed an onset desorption temperature decreased by 83 °C, reduced activation energy to 97.22 kJ/mol, and desorbed 6.35 wt% hydrogen within 20 min at 300 °C (Fig. 7H). Moreover, the hydrogen absorption capacity was stable at 97.8% after 20 cycles (Fig. 7I). The catalyst enhanced hydrogen cycling through the generation of Mg_2NiH_4 phases, effectively weakening Mg–H bonds, while Mo_2C provided stable active sites and promoted electron transfer, improving the kinetics of hydrogen desorption. Graphitized carbon further prevented particle aggregation and accelerated diffusion, markedly enhancing hydrogen storage performance (Fig. 7G).

MOF catalysts, relying on their ultra-large specific surface area, designable metal-ligand sites, and nano-confinement effects, can simultaneously achieve low-barrier H_2 cracking and hydrogen overflow, enhance electron transfer, and inhibit sintering. Shao et al. [82] demonstrated that thermally stable Ni-BTC300 MOF catalysts decreased hydrogen desorption barriers, enabling

MgH_2 doped with 10 wt% Ni-BTC300 to desorb 5.14 wt% hydrogen in 3 min at 300 °C, markedly higher than pure MgH_2 (0.09 wt%) under identical conditions. Li et al. [83] studied Ni-MOF@Pd catalysts, enhancing dehydrogenation through Mg_2Ni/Mg_2NiH_4-mediated hydrogen pumping and formation of Mg–Pd alloys. The composite's initial hydrogen desorption temperature was reduced to 181 °C. Lu et al. [84] reported that MOF–V catalysts reduced initial dehydrogenation temperature to 190.6 °C. During cycling, partial conversion to metallic vanadium enhanced interfacial catalysis and structural stability via nano-confinement effects.

Machine Learning and First-Principles Approaches for MgH_2 Hydrogen Storage

Current research on solid-state hydrogen storage catalysts rarely uses in situ techniques such as XRD or XAS (x-ray absorption spectroscopy) to explore phase transitions during cycling. This limits real-time insights into dynamic structures and hinders the rational design of more efficient catalyst systems. Recent advances in computation have placed density functional theory (DFT) and machine learning (ML) at the core of MgH_2-based hydrogen storage research. Combining experimental characterization with DFT and ML can shorten the trial-and-error cycle, provide atomic-level explanations for rate-limiting steps, and enable data-driven screening of complex composition-structure spaces. ML expands the scope of exploration to thousands, while DFT quantifies the thermodynamics and kinetics of active sites, which are ultimately verified by experimental characterization. The most effective strategy is to couple them into a single workflow for hypothesis generation, validation, and inverse design [85–89].

DFT studies have clarified key microscopic processes—including H_2 adsorption/dissociation, H diffusion, and Mg–H bond modulation—under realistic catalytic motifs (doping, interfacial alloys, and reconstructed surfaces). For example, Khajondetchairit et al. [90] showed that Ni/V decoration on Mg_2Ni surfaces enables barrierless H_2 dissociation via strong 3d–1s hybridization (Fig. 8A). It also reduces the H-diffusion barrier from 0.49 to 0.13 eV through bridged active sites and surface reconstruction (Fig. 8B and C). Reddad et al. [91] further demonstrated element-specific effects: Cu substitution markedly lowers the dehydrogenation barrier and temperature, whereas Zn showed limited impact due to insufficient orbital overlap with Mg. In another study, Didi et al. [92] examined ternary hydrides MgV_3H_8 and $MgFe_3H_8$ via CI-NEB calculations, identifying favorable phonon stability and low H-diffusion barriers (0.14 eV), though dehydrogenation temperatures above 599 K still exceeded DOE targets. Collectively, these studies show that DFT can (a) identify and tune active sites, (b) compute reaction and transport barriers, and (c) rationalize electronic-structure descriptors correlated with hydrogen kinetics. However, most models remain idealized, limiting transferability to real systems with nanoparticle agglomeration, by-product accumulation, and multielement synergies. The high computational cost of exhaustive sampling also constrains throughput.

ML has recently been adopted to overcome this bottleneck by learning structure–property relationships from computational and experimental data. Batalović et al. [93] developed the graph neural network model MetalHydrideEnth to screen over 600 Mg-containing intermetallics (Fig. 8D), identifying $MgBe_{13}$ as a lightweight and stable candidate (−42.5 kJ·mol^{-1} H_2 enthalpy) (Fig. 8E), and revealing atomic packing density as a structural descriptor strongly correlated with formation enthalpy (Fig. 8F). In another contribution, Dong et al. [94] established a supervised ML framework based on a curated database of 826 Mg-alloy hydride samples, training regression models with maximum hydrogen absorption and desorption as outputs. The GBR (gradient boosting regression) and MLP (multilayer perceptron) models achieved high accuracy (R^2 = 0.947 and 0.922). SHAP (Shapley Additive Explanations) analysis highlighted electronegativity mismatch, valence-electron concentration, and ball-milling parameters as critical descriptors for Mg-based hydrogen storage. The models successfully predicted promising candidates such as 96Mg–4Sm and 95Mg–1Ni–4Sm alloys, with hydrogen absorption and desorption capacities exceeding 6 wt% below 300 °C. Similarly, Jia et al. [95] used interpretable recurrent neural networks with SHAP analysis to identify milling time and processing temperature as key descriptors for $Mg(BH_4)_2$ composites, achieving dehydrogenation onset at 112.2 °C and 8.5 wt% capacity. These cases illustrate that ML can accelerate discovery, reveal hidden correlations, and guide synthesis. Yet, challenges persist: dataset scarcity, heterogeneous reporting standards, and limited physical interpretability often restrict generalization when ML is used alone.

The most promising path is the synergistic integration of DFT and ML. For instance, Li et al. [96] combined COHP (crystal orbital Hamiltonian population)-derived DFT descriptors with ML regressors, achieving <0.04 eV error in predicting dehydrogenation barriers of Ni/Mn-doped MgH_2 and identifying optimized doping pathways with barriers as low as 1.81 eV. Jiang et al. [97] used DFT to design NLi_4–B-doped graphene/MgH_2 heterojunctions, then integrated ML to screen 132 $Mg_{1-x}Me_xH_2$ alloys for tailored desorption temperatures. Validated candidates included $Mg_{0.875}Li_{0.125}H_2$ and $Mg_{0.875}Be_{0.125}H_2$ with 400 to 500 K desorption ranges. In another effort, Lee et al. [98] used a GAN (Generative Adversarial Network) to inverse-design 2D MgH_2 sheets; subsequent DFT uncovered a previously unknown P−4m2 phase. With Li decoration, it achieved 6 wt% gravimetric capacity and an adsorption energy of −0.105 eV. These hybrid approaches demonstrate how ML can explore broad compositional and structural spaces, while DFT validates physical mechanisms, enabling inverse design of Mg-based catalysts and heterostructures.

Looking forward, several directions deserve emphasis. First, unified databases integrating DFT outputs (energies, phonons, and diffusion paths) with standardized experimental data (activation energies, cycling metrics, and failure modes) are urgently needed. Second, physically informed ML models that encode symmetry, thermodynamic limits, and defect chemistry will enhance extrapolation reliability. Third, multiscale simulations bridging atomistic kinetics with mesoscale transport (grain growth and MgO/MgS by-products) and reactor-level performance will connect computational screening with real applications. Finally, applying integrated DFT–ML strategies to multicomponent and high-entropy catalysts in nano-confined carbon/oxide frameworks offers a pathway to cost-effective, durable MgH_2 systems that align with DOE targets. Overall, the convergence of DFT and ML should be considered not as auxiliary tools but as the central design engine for next-generation MgH_2 hydrogen storage catalysts.

Discussion

Figure 9 compiles several high-performance catalysts in this review. These systems typically couple rapid H_2 dissociation

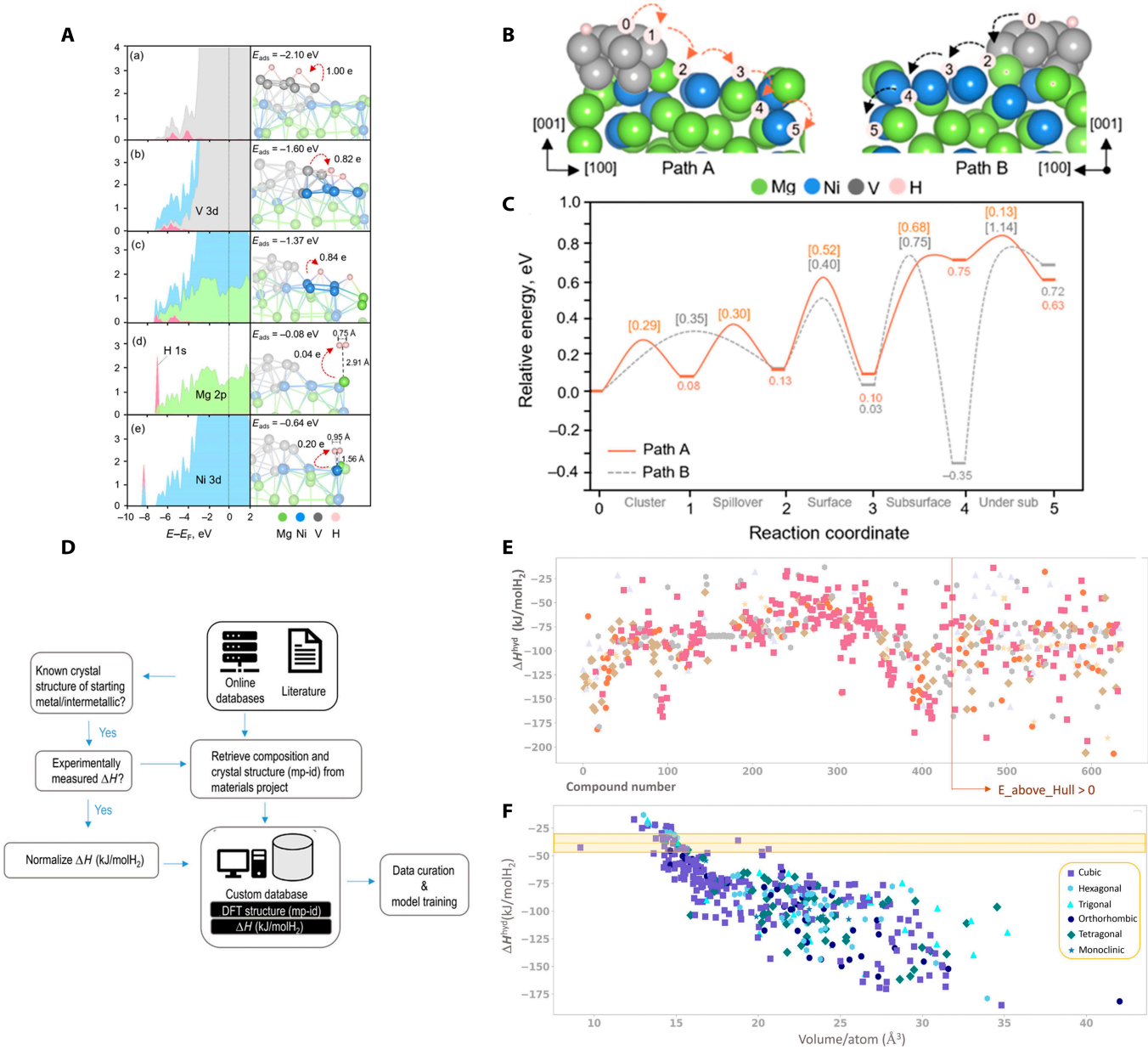


Fig. 8. (A) Projected density of states (PDOS) and atomic configurations of hydrogen adsorption at the V cluster, interface, hollow site, atop Mg, and atop Ni on the V_{10}/Mg_2Ni surface. (B) Atomic models of hydrogen diffusion along Path A and Path B from the V cluster to the under-subsurface region. (C) Reaction energy profiles corresponding to Path A and Path B, with diffusion barriers and relative energies labeled [90]. Reproduced with permission [90]. Copyright 2025, American Chemical Society. (D) MetalHydrideEnth model building process. (E) Distribution of predicted hydride formation enthalpies for 636 Mg-containing intermetallic compounds screened via the model. (F) Correlation between hydride formation enthalpy and atomic volume, highlighting a structural descriptor range favorable for near-ambient hydrogen storage (shaded area) [93].

with engineered Mg/MgH_2 interfaces, which shorten diffusion distances and preserve stability under repeated cycling.

High-entropy materials leverage dense local active sites, distortion-induced fast-diffusion channels, and the sintering resistance afforded by configurational entropy. As a result, they lower the barriers for both H_2 activation and Mg–H bond breaking/forming while sustaining interfacial activity. For example, with HELMO-NO_3 catalysis, MgH_2 absorbs 6.68 wt% hydrogen absorption within 3 min at 315 °C and 5.15 wt% at 75 °C. The MgH_2–FeCoNiCrMn alloy absorbs 5.5 wt% in 0.5 min at 150 °C and desorbs 5.8 wt% in 4 min at 280 °C, with 99% capacity retention after 50 cycles. Nonetheless, achieving and stabilizing near-atomic, single-phase solid solutions usually requires high-purity feedstocks and energy-intensive processing. These constraints raise manufacturing costs and narrow the practical window for scale-up.

Metal fluorides pair strong Lewis acidity with the in situ formation of fluorinated active surfaces. With K_2NbF_7, the MgH_2 composite shows a desorption activation energy of 96.3 kJ mol^{-1}, desorbs 5.2 wt% H_2 in 5.6 min at 320 °C, and still absorbs 4.7 wt% at 150 °C within 30 min. However, their preparation and use require strictly anhydrous handling and corrosion-resistant equipment. In humid environments, moisture-induced hydrolysis can generate HF, which shortens catalyst lifetime and adds nontrivial safety and environmental protection costs.

Single-atom and defect-engineered catalysts further accelerate kinetics: With $Ni@TiO_2$ catalysis, MgH_2 achieves 6.53 wt%

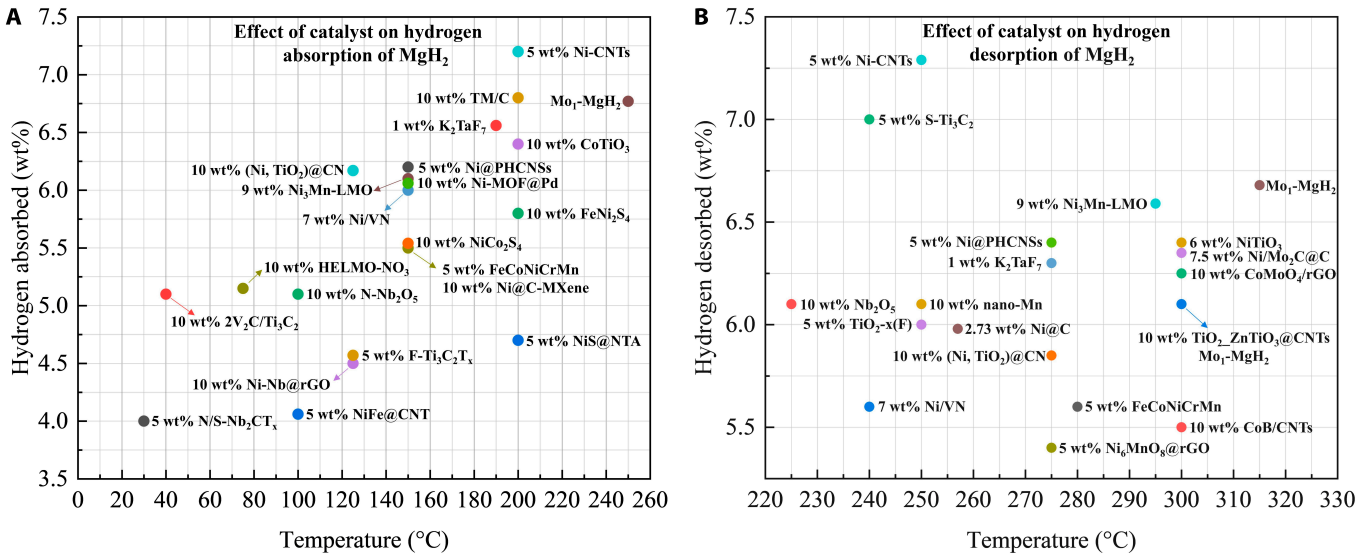


Fig. 9. The highly efficient catalysts' (A) hydrogen absorption and (B) hydrogen desorption.

absorption in 10 s and retains 97% capacity after 100 cycles. The activation energies drop to 64 kJ mol^{-1} (desorption) and 35 kJ mol^{-1} (absorption). Nevertheless, robust anchoring of isolated metal atoms at defect or coordination sites demands stringent control over precursors, atmosphere, and temperature. Such controls increase processing complexity and cost. Maintaining comparable defect densities and uniform single-atom dispersion at larger batch sizes remains challenging, and this currently limits reproducible manufacturing.

Carbon-based composites strike a favorable balance between activity and durability. The MgH_2–Sc_2O_3/TiO_2@graphene composite exhibits a dehydrogenation onset to 140 °C and maintains 99% capacity after 50 cycles. The MgH_2 composite catalyzed by ternary Ni–Nb/rGO exhibits a low apparent activation energy (57.8 kJ mol^{-1}), low-temperature absorption (2.75 wt% at 75 °C, 3 MPa, 30 min), and rapid desorption at moderate temperatures—benefits that derive from oxygen-vacancy chemistry, multiphase synergy, and rGO-assisted dispersion and transport. However, incorporating carbon-based composites at high loadings substantially dilutes the usable hydrogen-storage capacity. In addition, validation under high-density compaction conditions representative of on-board applications remains limited. The effects of the carbon framework on mass transport, heat conduction, and hydrogen absorption/desorption behavior under high pressure have not been systematically elucidated.

Collectively, these catalysts accelerate H_2 activation via defect-rich interfaces, Lewis-acid fluorides, single-atom sites, and conductive carbon scaffolds. However, challenges remain in scalable synthesis, cost, handling safety, and maintaining activity under practical conditions—issues that must be addressed for widespread application in hydrogen storage systems.

Conclusion

MgH_2 offers a gravimetric capacity of 7.6 wt% and is therefore an attractive solid hydrogen carrier. Its practical use, however, is constrained by high thermodynamic stability. Doped catalysts can reroute the reaction pathway and lower activation barriers. Through interfacial charge transfer, they weaken the Mg–H bond, thereby promoting H_2 dissociation, spillover, and atomic diffusion. During cycling, new interfacial phases often emerge—such as Mg_2Ni/Mg_2NiH_4, MgF_2, or MgS—producing multiphase architectures that suppress grain growth and preserve active surface area.

In recent years, several families of efficient catalysts have emerged to tackle the (de)hydrogenation-kinetics bottleneck of MgH_2. They promote interfacial charge transfer and band-structure modulation. They introduce defects and well-defined active sites. They also exploit nanoscale confinement. Representative systems include high-entropy catalysts, SACs, and carbon-based composite supports.

1. High-entropy catalysts utilize lattice distortion and multielement synergistic effects to promote interfacial electron transfer and weaken Mg–H bonds. The multielement composition provides abundant active sites and enhances both hydrogen absorption and desorption kinetics. Moreover, the intrinsic compositional disorder helps inhibit particle growth and maintains catalyst stability during cycling.
2. SACs operate via the "single atom–defect–support" interplay. Isolated metal atoms anchored on defects serve as highly active centers for hydrogen dissociation. The unique coordination environment and electronic interactions facilitate efficient charge transfer, sharply reducing activation energies without compromising the system's thermodynamic stability. Additionally, these catalysts offer tunable selectivity and enhanced durability by minimizing atom migration and aggregation.
3. Carbon-based matrices provide high surface area, electrical conductivity, and excellent dispersibility. The robust structural framework can host transition metal nanoparticles or single atoms, stabilizing them against sintering and aggregation. The conductive carbon matrix promotes fast electron transfer and can synergistically regulate hydrogen absorption and desorption kinetics.
4. Other types of catalysts discussed in this article, such as elemental metals, metal halides, metal sulfides, and metal carbides, have certain advantages in terms of material sources and preparation methods, and may play

a role in the initial large-scale hydrogen storage applications. However, their catalytic effects are relatively limited, and we look forward to further improvements in catalytic effects and cycle performance in the future.

Looking ahead, multielement high-entropy catalysts, SACs, and carbon-supported nanoscale confinement strategies are likely to be the mainstream research areas. Moreover, integrated, data-driven design paradigms will be crucial:

1. Co-ball milling MgH_2 with a high-entropy precursor to construct a multiphase, defect-rich contact interface in situ. During cycling, multicomponent species with variable valence states can be partially reduced, serving as both active sites and electron and hydrogen transport channels.
2. Anchoring transition metal single atoms onto a robust support (e.g., TiO_2 or fluoride nanosheets) achieves atomic-level dispersion and strong interfacial coupling, thereby promoting the H_2 cracking-escape-diffusion process and inhibiting grain coarsening.
3. Utilizing the dispersibility and stability of carbon materials to load nanoscale transition metal or solid solution nanoparticles, while simultaneously modulating thermodynamics and improving kinetics, enhances their cycling stability.
4. Combining in situ characterization, DFT, and ML can reveal dynamic structural evolution processes, predict reaction energies, and identify promising components before synthesis, thereby substantially reducing experimental costs and accelerating catalyst discovery and optimization.

Acknowledgments

Funding: This work was partially supported by the Special Fund Project of Carbon Peaking Carbon Neutrality Science and Technology Innovation of Jiangsu Province (BE2022011), the Carbon Peaking Carbon Neutrality Science and Technology Innovation of Nanjing City (202211016), the National Natural Science Foundation of China (No. 52172249), the Funding of Nanjing Institute of Future Energy System (KCW-12), the Chinese Academy of Sciences Talents Program (E2290701), and the Jiangsu Province Talents Program (JSSCRC2023545).
Author contributions: Y.Z. performed the literature review and drafted the manuscript. W.M. assisted in the collection and organization of relevant literature. X.C., Y.G., and W.W. contributed to the in-depth review and provided constructive feedback. H.C. and T.Z. supervised the work. All authors discussed the results and contributed to the final revision of the manuscript.
Competing interests: The authors declare that they have no competing interests.

Supplementary Materials

Tables S1 to S8

References

1. Zheng J, Wang CG, Zhou H, Ye E, Xu J, Li Z, Loh XJ. Current research trends and perspectives on solid-state nanomaterials in hydrogen storage. *Research*. 2021;2021:Article 3750689.
2. Xiao H, Qian F, Zhang X, Hu H, Tang R, Hu C, Zhou W, He X, Pu Z, Ma C, et al. Effect of $Ce_{0.6}Zr_{0.4}O_2$ nanocrystals on boosting hydrogen storage performance of MgH_2. *Chem Eng J*. 2024;494:Article 153203.
3. Wang P, Tian Z, Wang Z, Xia C, Yang T, Ou X. Improved hydrogen storage properties of MgH_2 using transition metal sulfides as catalyst. *Int J Hydrog Energy*. 2021;46(53):27107–27118.
4. Ye Y, Zhang Z, Liu J, Yan K, Wang W, Cheng H. Experiment and simulation study on transfer phenomena and performance optimization of MgH_2 based hydrogen storage reactors. *Int J Hydrog Energy*. 2024;86:649–661.
5. Zhang J, Yan S, Xia G, Zhou X, Lu X, Yu L, Yu X, Peng P. Stabilization of low-valence transition metal towards advanced catalytic effects on the hydrogen storage performance of magnesium hydride. *J Magnesium Alloys*. 2021;9(2):647–657.
6. Sazelee NA, Ali NA, Yahya MS, Din MM, Ismail M. Enhancing hydrogen storage performance of MgH_2 through the addition of $BaMnO_3$ synthesized via solid-state method. *Int J Hydrog Energy*. 2023;48(79):30844–30857.
7. Fu Y, Zhang L, Li Y, Guo S, Yu H, Wang W, Ren K, Zhang W, Han S. Effect of ternary transition metal sulfide $FeNi_2S_4$ on hydrogen storage performance of MgH_2. *J Magnesium Alloys*. 2023;11(8):2927–2938.
8. Wang L, Zhang L, Wu F, Jiang Y, Yao Z, Chen L. Promoting catalysis in magnesium hydride for solid-state hydrogen storage through manipulating the elements of high entropy oxides. *J Magnesium Alloys*. 2024;12(12):5038–5050.
9. Le TT, Pistidda C, Singh P, Raizada P, Klassen T, Dornheim M. Nanoconfinement effects on hydrogen storage properties of MgH_2 and $LiBH_4$. *Int J Hydrog Energy*. 2021;46(46):23723–23736.
10. Paul B, Kumar S, Majumdar S. Preparation, characterization and modification of magnesium hydride for enhanced solid-state hydrogen storage properties. *Int J Hydrog Energy*. 2024;96:494–501.
11. Wang L, Zhang L, Lu X, Wu F, Sun X, Zhao H, Li Q. Surprising cocktail effect in high entropy alloys on catalyzing magnesium hydride for solid-state hydrogen storage. *Chem Eng J*. 2023;465:Article 142766.
12. Zhu Y, Qin Z, Shi X, Ding X, Dao VD, Li Y. Size-dependent activity modulation of supported Ni nanocatalysts for efficient solid-state hydrogen storage in magnesium. *Chem Eng J*. 2024;498:Article 155285.
13. Zhang L, Cai Z, Yao Z, Ji L, Sun Z, Yan N, Zhang B, Xiao B, du J, Zhu X, et al. A striking catalytic effect of facile synthesized $ZrMn_2$ nanoparticles on the de/rehydrogenation properties of MgH_2. *J Mater Chem A*. 2019;7(10):5626–5634.
14. Xin DI, Ruirun CH, Xiaoyu CH, Wenchao CA, Hongsheng DI, Yanqing SU, Jingjie GU. De-/hydrogenation mechanism of Mg-based hydrogen storage alloys and their microstructure and property control. *Chin J Nat*. 2020;42(3):179–186.
15. Assila A, Belkoufa I, Rkhis M, Alaoui-Belghiti A, Laasri S, Hlil EK, Hajjaji A. Unlocking the hydrogen storage characteristics of MgH_2 hydrides: Investigating the impact of mechanical strain and substitutions. *J Energy Storage*. 2025;122:Article 116708.
16. Gao D-Q, Wu F-Y, Zhang Z, Lu Z-C, Zhou R, Zhao H, Zhang L-T. Graphene-loaded nickel–vanadium bimetal oxides as hydrogen pumps to boost solid-state hydrogen storage kinetic performance of magnesium hydride. *Trans Nonferrous Metals Soc China*. 2024;34(8):2645–2657.

17. Liu Y, Wang C, Song Y, Li Z, Wang X, Qi F, Chen J, Liu Y, Gao M, Pan H. Reduced graphene oxide/patronite composite as highly active catalyst precursors for enhancing the hydrogen desorption of MgH_2. *J Magnesium Alloys*. 2025.
18. Zhang Q, Du S, Ma Z, Lin X, Zou J, Zhu W, Ren L, Li Y. Recent advances in Mg-based hydrogen storage materials. *Chin Sci Bull*. 2021;67(19):2158–2171.
19. Zhang L, Zhang X, Zhang W, Fang F, Li J, Hu J, Gu C, Sun W, Gao M, Pan H, et al. In situ creation of a catalytic multiphase and multiscale surroundings for remarkable hydrogen storage performance of MgH_2. *J Mater Chem A*. 2024;12(4):2423–2434.
20. Yan CH, Zhang HY, Ze SU, Zheng JG, Zhang LT. Mn nanoparticles enhanced dehydrogenation and hydrogenation kinetics of MgH_2 for hydrogen storage. *Trans Nonferrous Metals Soc China*. 2021;31(11):3469–3477.
21. Yang C, Hu C, Wu X, Pang Y, Liu X, Shui J. Alloy-type Mo single-atom catalyst enhancing hydrogen storage performance of MgH_2. *J Energy Chem*. 2025;105:185–192.
22. Yang X, Ji L, Yan N, Sun Z, Lu X, Zhang L, Zhu X, Chen L. Superior catalytic effects of FeCo nanosheets on MgH_2 for hydrogen storage. *Dalton Trans*. 2019;48(33):12699–12706.
23. Wan H, Yang X, Zhou S, Ran L, Lu Y, Chen YA, Wang J, Pan F. Enhancing hydrogen storage properties of MgH_2 using FeCoNiCrMn high entropy alloy catalysts. *J Mater Sci Technol*. 2023;149:88–98.
24. Jiang Y, Liu Y, Yue M, Sun Y, Cao Y, Yuan Q, Wang Y. Pulsed electrodeposited rare earth medium-entropy amorphous alloys for catalyzing MgH_2 for solid-state hydrogen storage. *J Energy Storage*. 2025;107:Article 114956.
25. Huang Y, An C, Zhang Q, Zang L, Shao H, Liu Y, Zhang Y, Yuan H, Wang C, Wang Y. Cost-effective mechanochemical synthesis of highly dispersed supported transition metal catalysts for hydrogen storage. *Nano Energy*. 2021;80:Article 105535.
26. Machmud MN, Jalil Z. Sorption behavior of MgH_2-Ti for hydrogen storage material prepared by high pressure milling. *J Phys Conf Ser*. 2021;1882(1):Article 012005.
27. Rahwanto A, Ismail I, Nurmalita N, Mustanir, Jalil Z. Nanoscale Ni as a catalyst in MgH_2 for hydrogen storage material. *J Phys Conf Ser*. 2021;1882(1):Article 012010.
28. Pereira AD, Paciornik S, Santos DS, Jardim PM. Characterization of TiO_2 nanoparticle's morphology and its influence on the hydrogen sorption kinetics of MgH_2. *Mater Res*. 2019;22(Suppl 1):Article e20180821.
29. Ma Z, Liu J, Zhu Y, Zhao Y, Lin H, Zhang Y, Li H, Zhang J, Liu Y, Gao W, et al. Crystal-facet-dependent catalysis of anatase TiO_2 on hydrogen storage of MgH_2. *J Alloys Compd*. 2020;822:153553–152559.
30. Zhang J, Wang W, Chen X, Jin J, Yan X, Huang J. Single-atom Ni supported on TiO_2 for catalyzing hydrogen storage in MgH_2. *J Am Chem Soc*. 2024;146(15):10432–10442.
31. Wang K, Zhang X, Ren Z, Zhang X, Hu J, Gao M, Pan H, Liu Y. Nitrogen-stimulated superior catalytic activity of niobium oxide for fast full hydrogenation of magnesium at ambient temperature. *Energy Storage Mater*. 2019;23:79–87.
32. Liang H, Xie Z, Zhao R, Wen X, Hong F, Shi W, Chen H, Liu H, Zhou W, Guo J, et al. Facile synthesis of nickel-vanadium bimetallic oxide and its catalytic effects on the hydrogen storage properties of magnesium hydride. *Int J Hydrog Energy*. 2022;47(77):32969–32980.
33. Zhang J, Hou Q, Guo X, Yang X. Achieve high-efficiency hydrogen storage of MgH_2 catalyzed by nanosheets $CoMoO_4$ and rGO. *J Alloys Compd*. 2022;911:165153–165165.
34. Zhong T, Xu T, Zhang L, Wu F, Jiang Y, Yu X. Designing multivalent NiMn-based layered nanosheets with high specific surface area and abundant active sites for solid-state hydrogen storage in magnesium hydride. *J Magnesium Alloys*. 2025;13(1):148–160.
35. Wang L, Zhong T, Wu F, Chen D, Yao Z, Chen L, Zhang L. Anions intercalated two-dimension high entropy layered metal oxides for enhanced hydrogen storage in magnesium hydride. *Chem Eng J*. 2025;505:Article 159591.
36. Ismail M. Effect of adding different percentages of $HfCl_4$ on the hydrogen storage properties of MgH_2. *Int J Hydrog Energy*. 2021;46(12):8621–8628.
37. Suárez-Alcántara K, Flores-Jacobo NI, Osorio-García MD, Cabañas-Moreno JG. Fast hydrogen sorption kinetics in Mg-VCl_3 produced by cryogenic ball-milling. *Materials*. 2023;16(6):Article 2526.
38. Ismail M. Effect of $LaCl_3$ addition on the hydrogen storage properties of MgH_2. *Energy*. 2015;79:177–182.
39. Ismail M, Mustafa NS, Juahir N, Yap FH. Catalytic effect of $CeCl_3$ on the hydrogen storage properties of MgH_2. *Mater Chem Phys*. 2016;170:77–82.
40. Yahya MS, Sulaiman NN, Mustafa NS, Yap FH, Ismail M. Improvement of hydrogen storage properties in MgH_2 catalysed by K_2NbF_7. *Int J Hydrog Energy*. 2018;43(31):14532–14540.
41. Yan C, Lu X, Zheng J, Zhang Y, Wu Q, Wu F, Zhang L. Dual-cation K_2TaF_7 catalyst improves high-capacity hydrogen storage behavior of MgH_2. *Int J Hydrog Energy*. 2023;48(15):6023–6033.
42. Yusnizam NY, Ali NA, Sazelee NA, Nasef MM, Jalil AA, Ismail M. Boosting the de-/rehydrogenation properties of MgH_2 with the addition of $BaCoF_4$. *J Alloys Compd*. 2023;967:171618–171625.
43. Zhu L, Liao Y, Zhong Y, Cui J, Wang D, Wang K. Improved reversible dehydrogenation performance of MgH_2 by the synergistic effects of porous boron nitride and NbF_5. *J Energy Storage*. 2020;29:101418–101424.
44. Shi Q, Gao Y, Zhao S, Zhang C, Liu C, Wang C, Wang S, Li Y, Yin D, Wang L, et al. Interfacial engineering of fluorinated TiO_2 Nanosheets with abundant oxygen vacancies for boosting the hydrogen storage performance of MgH_2. *Small*. 2024;20(18):2307965.
45. Zhang T, Liu M, Li C, Zhang J, Gao H, Kong F, Xiao X. Synergistic catalysis of YF_3 and Ni/C: Exceptional effects on hydrogen storage performances of MgH_2 at low temperature. *Chem Eng J*. 2025;511:Article 162185.
46. Cheng Y, Bi J, Zhang W. The hydrogen storage properties of MgH_2–Fe_7S_8 composites. *Mater Adv*. 2021;2(2):736–742.
47. Xie X, Xiao L, Kimura H, Wu P, Du W, Wu Y. Effects of layered walnut NiS@NTA on hydrogen storage performance of MgH_2. *Sep Purif Technol*. 2025;359:Article 130837.
48. Tan D, Peng C, Zhang Q. Microstructural characteristics and hydrogen storage properties of the Mg–Ni–TiS_2 nanocomposite prepared by a solution-based method. *Int J Hydrog Energy*. 2023;48(44):16756–16768.
49. Chen Y, Sun B, Zhang G, Wang Y, Li X. Catalytic effect of double transition metal sulfide $NiCo_2S_4$ on hydrogen storage properties of MgH_2. *Appl Surf Sci*. 2024;645:Article 158801.
50. Fu Y, Zhang L, Li Y, Guo S, Yu Z, Wang W, Ren K, Peng Q, Han S. Catalytic effect of MOF-derived transition metal catalyst FeCoS@C on hydrogen storage of magnesium. *J Mater Sci Technol*. 2023;138:59–69.

51. Zheng L, Li S, Zhang L, Zhong T, Wang X, Bian T, Senin P, Wu Y. A MOF derived multi-phase $FeNi_3$-S catalyst for efficient hydrogen storage in magnesium hydride. *Chin Chem Lett*. 2024;110414.
52. Yuan Z, Zhang X, Wu Y, Guan S, Zhao S, Ji L, Peng Q, Han S, Fan Y, Liu B. Effectively enhanced catalytic effect of sulfur doped Ti_3C_2 on the kinetics and cyclic stability of hydrogen storage in MgH_2. *J Magnesium Alloys*. 2025;13(4):1843–1853.
53. Liu M, Zhao S, Xiao X, Chen M, Sun C, Yao Z, Hu Z, Chen L. Novel 1D carbon nanotubes uniformly wrapped nanoscale MgH_2 for efficient hydrogen storage cycling performances with extreme high gravimetric and volumetric capacities. *Nano Energy*. 2019;61:540–549.
54. Duan C, Tian Y, Wang X, Wu M, Fu D, Zhang Y, Lv W, Su Z, Xue Z, Wu Y. Ni-CNTs as an efficient confining framework and catalyst for improving dehydriding/rehydriding properties of MgH_2. *Renew Energy*. 2022;187:417–427.
55. Lu X, Yang X, Liang X, Hou Q, Kong J, Su J. TiO_2_$ZnTiO_3$ with carbon nanotubes catalytically improve the hydrogen storage characteristics of MgH_2. *J Power Sources*. 2024;623:Article 235455.
56. Fu Y, Yu Z, Guo S, Li Y, Peng Q, Zhang L, Wu S, Han S. Catalytic effect of bamboo-like carbon nanotubes loaded with NiFe nanoparticles on hydrogen storage properties of MgH_2. *Chem Eng J*. 2023;458:Article 141337.
57. Wan H, Qiu J, Guan H, Ding Z, Lu Y, Chen YA, Wang J, Pan F. FCC/α-Fe biphasic nano-sites synergize with CNTs to enhance reversible hydrogen storage of MgH_2. *Inorg Chem Front*. 2024;11(14):4197–4206.
58. Duan C, Wang H, Wu J, Qu T, Zhang Y, Fu D, Hu L, Wang F, Lai D, Dai Y, et al. Co@Pd bimetallic catalysts doped on the CNTs for bidirectional improving hydriding/dehydriding property of Mg/MgH_2. *J Energy Storage*. 2024;91:Article 112015.
59. Ren L, Zhu W, Zhang Q, Lu C, Sun F, Lin X, Zou J. MgH_2 confinement in MOF-derived N-doped porous carbon nanofibers for enhanced hydrogen storage. *Chem Eng J*. 2022;434:134701–134711.
60. Hu JQ, Jiang W, Si N, Wang Z, Zhang H. MOF-derived carbon supported transition metal (Fe, Ni) and synergetic catalysis for hydrogen storage kinetics of MgH_2. *Int J Hydrog Energy*. 2024;86:445–455.
61. Huang H, Chen J, Xu T, Lv Y, Liu B, Zhang B, Yuan J, Wu Y. Graphene-supported Sc_2O_3/TiO_2 for superior catalysis on hydrogen sorption kinetics of MgH_2. *Energy Mater Adv*. 2023;4:0055.
62. Verma SK, Bhatnagar A, Shukla V, Soni PK, Pandey AP, Yadav TP, Srivastava ON. Multiple improvements of hydrogen sorption and their mechanism for MgH_2 catalyzed through TiH_2@gr. *Int J Hydrog Energy*. 2020;45(38):19516–19530.
63. Song M, Zhang L, Zheng J, Yu Z, Wang S. Constructing graphene nanosheet-supported FeOOH nanodots for hydrogen storage of MgH_2. *Int J Miner Metall Mater*. 2022;29(7):1464–1473.
64. Guemou S, Zhang L, Li S, Jiang Y, Zhong T, Lu Z, Zhou R, Wu F, Li Q. Exceptional catalytic effect of novel rGO-supported Ni-Nb nanocomposite on the hydrogen storage properties of MgH_2. *J Mater Sci Technol*. 2024;172:83–93.
65. Li J, Wang S, Du Y, Liao W. Catalytic effect of Ti_2C MXene on the dehydrogenation of MgH_2. *Int J Hydrog Energy*. 2019;44(13):6787–6794.
66. Liu H, Lu C, Wang X, Xu L, Huang X, Wang X, Ning H, Lan Z, Guo J. Combinations of V_2C and Ti_3C_2 MXenes for boosting the hydrogen storage performances of MgH_2. *ACS Appl Mater Interfaces*. 2021;13(11):13235–13247.
67. Lu H, Li J, Zhou X, Lu Y, Chen YA, Li Q, Pan F. N/S co-doped Nb_2CT MXene as the effective catalyst for improving the hydrogen storage performance of MgH_2. *J Mater Sci Technol*. 2024;190:135–144.
68. Zhu W, Ren L, Li Y, Lu C, Lin X, Zhang Q, Yang X, Hu Z, Cheng T, Zhao Y, et al. In situ high-energy synchrotron X-ray studies in thermodynamics of Mg-in-Ti hydrogen storage system. *Energy Mater Adv*. 2023;4:0069.
69. Lan Z, Hong F, Shi W, Zhao R, Li R, Fan Y, Liu H, Zhou W, Ning H, Guo J. Effect of MOF-derived carbon–nitrogen nanosheets co-doped with nickel and titanium dioxide nanoparticles on hydrogen storage performance of MgH_2. *Chem Eng J*. 2023;468:Article 143692.
70. Wang Y, Ding Z, Li X, Ren S, Zhou S, Zhang H, Li Y, Han S. Improved hydrogen storage properties of MgH_2 by nickel@nitrogen-doped carbon spheres. *Dalton Trans*. 2020;49(11):3495–3502.
71. Wang S, Gao M, Yao Z, Xian K, Wu M, Liu Y, Sun W, Pan H. High-loading, ultrafine Ni nanoparticles dispersed on porous hollow carbon nanospheres for fast (de)hydrogenation kinetics of MgH_2. *J Magnesium Alloys*. 2022;10(12):3354–3366.
72. Soni PK, Bhatnagar A, Shaz MA. Enhanced hydrogen properties of MgH_2 by Fe nanoparticles loaded hollow carbon spheres. *Int J Hydrog Energy*. 2023;48(47):17970–17982.
73. Cheng H, Chen G, Zhang Y, Zhu Y, Li L. Boosting low-temperature de/re-hydrogenation performances of MgH_2 with Pd-Ni bimetallic nanoparticles supported by mesoporous carbon. *Int J Hydrog Energy*. 2019;44(21):10777–10787.
74. Yu H, Cheng Y, Fu Y, Zhang L, Guo S, Li Y, Zhang W, Han S. Remarkable hydrogen properties of MgH_2 via combination of an in-situ formed amorphous carbon. *Int J Hydrog Energy*. 2022;47(68):29358–29370.
75. Zhou D, Cui K, Zhou Z, Liu C, Zhao W, Li P, Qu X. Enhanced hydrogen-storage properties of MgH_2 by Fe–Ni catalyst modified three-dimensional graphene. *Int J Hydrog Energy*. 2021;46(69):34369–34380.
76. Li F, Huang Z, Wang Y, Wu L, Guan S, Wang Y, Liu Y, Cheng S, Wu J, Hu J, et al. Effect of MOF-derived nanoparticle-cumulated flower-like CoFe@C coated composites on hydrogenation/dehydrogenation performance of MgH_2. *Chem Eng J*. 2024;485:150008–115021.
77. Guo S, Yu Z, Li Y, Fu Y, Zhang Z, Han S. Preparation of Mg-Mg_2Ni/C composite and its excellent hydrogen storage properties. *J Alloys Compd*. 2024;976:173035–117043.
78. Sun W, Zhang H, He Q, Zhang R, Wu J, Wang Y, Bu Y, Li B, Sun L, Xu F, et al. Monolithic nickel-doped molybdenum nitride improves hydrogen storage properties of MgH_2. *J Alloys Compd*. 2025;1010:177000–177010.
79. Wu J, Liu Z, Zhang H, Zou Y, Li B, Xiang C, Sun L, Xu F, Yu T. Hydrogen storage performance of MgH_2 under catalysis by highly dispersed nickel-nanoparticle–doped hollow spherical vanadium nitride. *J Magnesium Alloys*. 2024;12(12):5132–5143.
80. Yao L, Lyu X, Zhang J, Liu Y, Zhu Y, Lin H, Zhang Y, Li L. Remarkable synergistic effects of Mg_2NiH_4 and transition metal carbides (TiC, ZrC, WC) on enhancing the hydrogen storage properties of MgH_2. *Int J Hydrog Energy*. 2020;45(11):6765–6779.
81. Yuan Q, Peng C, Yang C, Li Y, Zhang Q, Lv Y, Liu G, Liu D. Facilitated hydrogen storage properties of MgH_2 by Ni

nanoparticles anchored on Mo_2C@C nanosheets. *Int J Hydrog Energy*. 2024;85:12–19.
82. Shao H, Huang Y, Guo H, Liu Y, Guo Y, Wang Y. Thermally stable Ni MOF catalyzed MgH_2 for hydrogen storage. *Int J Hydrog Energy*. 2021;46(76):37977–37985.
83. Li ZY, Sun LX, Xu F, Luo YM, Xia YP, Wei S, Zhang CC, Cheng RG, Ye CF, Liu MY, et al. Modulated noble metal/2D MOF heterostructures for improved hydrogen storage of MgH_2. *Rare Metals*. 2023;43(4):1672–1685.
84. Lu Z, He J, Song M, Zhang Y, Wu F, Zheng J, Zhang L, Chen L. Bullet-like vanadium-based MOFs as a highly active catalyst for promoting the hydrogen storage property in MgH_2. *Int J Miner Metall Mater*. 2022;30(1):44–53.
85. Liu D, Liu Z, Zhang J, Yin Y, Xi J, Wang L, Xiong JF, Zhang M, Zhao T, Jin J, et al. Classification and prediction of Skyrmion material based on machine learning. *Research*. 2023;6:0082.
86. Fan M, Sang C, Li H, Wei Y, Zhang B, Xing Y, Zhang J, Yin J, An W, Shao B. Development of an efficient and generalized MTSCAM model to predict liquid chromatography retention times of organic compounds. *Research*. 2025;8:Article 0607.
87. Jiao L, Wang Y, Liu X, Li L, Liu F, Ma W, Guo Y, Chen P, Yang S, Hou B. Causal inference meets deep learning: A comprehensive survey. *Research*. 2024;7:Article 0467.
88. Arharbi A, Jebari H, Ez-Zahraouy H. New insights from DFT analysis: Mg vacancies and hydrogen doping in enhancing thermodynamic properties and hydrogen storage performance of Li_2BeMgH_6. *J Energy Storage*. 2025;106:Article 114903.
89. Zhou P, Zhou Q, Xiao X, Fan X, Zou Y, Sun L, Jiang J, Song D, Chen L. Machine learning in solid-state hydrogen storage materials: Challenges and perspectives. *Adv Mater*. 2025;37(6):2413430.
90. Khajondetchairit P, Ngamwongwan L, Hirunsit P, Suthirakun S. Synergistic effects of V and Ni catalysts on hydrogen sorption kinetics of Mg-based hydrogen storage materials: A computational study. *J Phys Chem C*. 2022;126(12):5483–5492.
91. Reddad K, Labrim H, Zejli D, El Bouayadi R. Enhancing hydrogen desorption in MgH_2: A DFT study on the effects of copper and zinc doping. *Int J Hydrog Energy*. 2024;87:1474–1479.
92. Didi Y, El Fatouaki Z, Touti R, Ahfir R, Tahiri A, Naji M, Idiri M, Rjeb A. First principles computational study of MgX_3H_8 (X=V and Fe) for hydrogen storage applications. *Int J Hydrog Energy*. 2025;133:140–151.
93. Batalović K, Radaković J, Kuzmanović B, Ilić MM, Mamula BP. Machine learning-based high-throughput screening of Mg-containing alloys for hydrogen storage and energy conversion applications. *J Energy Storage*. 2023;68:Article 107720.
94. Dong S, Wang Y, Li J, Li Y, Wang L, Zhang J. Exploration and design of Mg alloys for hydrogen storage with supervised machine learning. *Int J Hydrog Energy*. 2023;48(97):38412–38424.
95. Jia Y, Fang H, Chen L, Han B, Tang L, Wang J, Xia Y, Zou Y, Sun L, Li H, et al. Interpretable machine learning enables high performance of magnesium borohydride hydrogen storage system. *J Magnesium Alloys*. 2025;13(9):4430–4445.
96. Li C, Yang W, Liu H, Liu X, Xing X, Gao Z, Dong S, Li H. Picturing the gap between the performance and US-DOE'S hydrogen storage target: A data-driven model for MgH_2 dehydrogenation. *Angew Chem Int Ed Engl*. 2024;63(28):Article e202320151.
97. Jiang Q, Jia Z, Lu S, Song P, Gao Z, Wang Z, Peng T, Bai X, Cui H, Tian W, et al. Novel NLi_4-BGra/MgH_2-based heterojunctions for efficient hydrogen storage and modulation of hydrogen-desorption temperature ranges. *Ceram Int*. 2024;50(13):23058–23069.
98. Lee J, Sung D, Chung YK, Song SB, Huh J. Unveiling two-dimensional magnesium hydride as a hydrogen storage material via a generative adversarial network. *Nanoscale Adv*. 2022;4(10):2332–2338.